THE EXHUMATION OF CONTINENTAL CRUST IN COLLISIONAL BELTS: INSIGHTS FROM THE DEEP STRUCTURE OF ALPINE CORSICA IN THE CIMA PEDANI AREA.

Maria Di Rosa[1,2], Francesca Meneghini[1*], Michele Marroni[1,3], Noah Hobbs[1], Olivier Vidal[4]

1 Dipartimento di Scienze della Terra, Università di Pisa, Italy
2 Dipartimento di Scienze della Terra, Università di Firenze, Italy
3 Istituto di Geoscienze e Georisorse, IGG-CNR, Pisa, Italy
4 IsTerre, CNRS, Grenoble, France

==========
* CORRESPONDING AUTHOR:
Dr. MARIA DI ROSA,
DIPARTIMENTO DI SCIENZE DELLA TERRA,
UNIVERSITÀ DI PISA, VIA S. MARIA, 53
56126 PISA, ITALY.
E-MAIL: maria.dirosa@unifi.it

ABSTRACT

In the northern Corsica, the Cima Pedani area is characterized by a stack of continental and oceanic units belonging to the Alpine Corsica. The base of the units stack consists of three metamorphic continental units (Canavaggia, Pedani and Scoltola Units) that are overthrust by the Schistes Lustrés Complex, represented by oceanic units. The continental units are metamorphic fragments of the European continental margin. They include a Paleozoic basement intruded by Permo-Carboniferous metagranitoids covered by a Permian metavolcanites and a Triassic-Jurassic metacarbonatic sequence, unconformably covered by metabreccias and metasandstones of the Eocene age. These units are affected by a polyphased tectono-metamorphic history acquired in a time lapse running from Priabonian to Aquitanian. The reconstructed P-T paths and the related deformations describe a retrograde history acquired during their progressive exhumation, whereas no trace of the older prograde history has been ~~con~~preserved. In all the reconstructed P-T paths, the P-peak corresponds to the maximum depth reached by these units (i.e. 1.04 - 1.35 GPa), whereas the subsequent history includes a progressive P decrease associated to coeval T increase. The deformation history related to exhumation includes three deformation phases. In particular, the D2 phase is characterized by non-coaxial ductile structures parallel to the boundaries of the units observed in the Cima Pedani tectonic window. The sense of shear of these shear zones is generally top-to-the W, i.e. toward the Alpine foreland. The collected data provide the evidence that the continental units were deformed and metamorphosed during the

exhumation following their ascent path along the plate boundary interface. The geodynamic mechanism we proposed for the exhumation of the Cima Pedani units is the subduction channel, in which HP units arise between the downgoing plate and the former accretionary wedge built-up during the oceanic subduction, represented by the Schistes Lustrés Complex.

1. INTRODUCTION

Underthrusting of continental crust is a natural fate of oceanic subduction in convergent margins. Several modeling studies have shown the various conditions that can make continental crust prone to subduction (Cloos 1982; Chemenda et al. 1995; 1996; Ernst 2001), and several evidences from exhumed orogens show that continental crust can be underthrust down to depths > 50 km so that they deform under eclogite facies, giving rise to high-pressure and ultra high-pressure (HP and UHP, respectively) units (Chopin 1984; Dewey et al. 1993; Chemenda et al. 1996; Compagnoni and Rolfo 2003; Ernst 2001; 2005; Guillot et al. 2009).

The vertical movement of continental slices from depth up to the surface is far from ~~to be~~ clearly understood, and different mechanisms have been proposed for the exhumation of HP and UHP units in orogenic belts, including the "classic", but worthy to note models such as channel flow (Cloos 1982), corner flow (Platt 1986), extensional collapse (Dewey et al. 1993), thrusting onto the foreland (Steck et al. 1998), buoyancy through erosion and tectonic processes (Polino et al. 1990), compression of a soft zone between two rigid blocks (Thompson et al. 1997), serpentinite channel (Guillot et al. 2001), early fast exhumation at depth followed by slow exhumation below extensional detachments (Jolivet et al. 2003) and extraction of rock volumes resulting from the merging of two block-bounding faults with opposite senses of displacement (i.e. extraction faults described by Froitzheim et al., 2006). The development of different tectonic regimes during continental subduction depends, as for extensional and compressional regimes during oceanic

subduction, on factors such as the pull force, the plate convergent rate and the geothermal gradient, that can change dramatically when continental crust enters the subduction zone and, progressively, during the proceeding of continental subduction. Consequently, the style of deformation, the metamorphic conditions and the exhumation mechanisms of HP continental rocks can change with time even in a single margin. The diverse possible mechanisms of exhumation developed through different thermomechanical processes testify the critical role of deciphering the kinematic evolution and dating the metamorphic history of HP continental units in orogenic belts (e.g. Guillot et al., 2009).

The Alpine Corsica, i.e. the geological domain that occupy the northeastern side of the island (Fig.1a), consists of a complex stack of continental and oceanic units of a variable degree of metamorphism from very low-grade to blueschist-eclogite facies, that are interpreted as the southward extension of the Western Alps collisional belt (e.g. Mattauer et al. 1981; Durand-Delga 1984). As in the Western Alps, the units with continental affinity are overthrust by oceanic and transitional units, referred to as the Schistes Lustrés Complex (Gibbons et al. 1986; Caron 1994; Levi et al. 2007; Vitale Brovarone et al. 2013). Continental units crop out along a north-south trending strip at the western border of the Alpine Corsica (Fig.1a) and are regarded as fragments of the thinned European margin (Durand-Delga 1984; Caron 1994; Malasoma et al. 2006; Molli et al. 2006; Di Rosa et al. 2017a) that underwent Early Cenozoic continental subduction, and subsequent syn-convergent exhumation, as a result of the closure of western Tethys (Amaudric du Chaffaut and Saliot 1979; Caron 1994; Malasoma and Marroni

=CL ECCLS Daa4ECCÀyT 411 s i Fah sDr F3 , F si aR, mF3 , 3DsF i 4 2 n FD

=CÀ Di c s2 i , FDRR 4 aR4 Ds, 4 ns4 2 sah a42D i 1 3 naF FaT

=CY =YÀ: S Da4c F FaT=YYCS Dnsi 4 s F aT=YY=S sni F FaTECCCym F3n,

==C aaDe 4 2 FF s Rs , sc F4Di D1 F3 aR4 Daa4 4Di a Fsn Fns , T

===

s RDsF 3 s Di e aaU gRD, , F4Di F3sDn23 g3nr P

==E r F r DsR34 Di F4 i Fa hi 4F, mF3 D2i 4* 4 F FDi 4 e 4 De DnF sDRR4 2

==A 4 F3 4r i 4 s mF F3 Dni sh Fe i F3 aR4 i F3 s4 i

==: , FDs, D1 Ds, 4 I 42'T=yT 1F s 1s r 4 2 F3 s 4 F3 aR4 Ds, 4

==. s 24Di a, FF4 2m e Rs , i F F3 s , naF, D1 F 4a , Fsn Fns a i

==Z 1Dsr F4Di i ah, 4, Di n F Di F3 , hi 4F, mDnRa e 4F3 i , F4r F D1

==L F3 U Di 4F4Di , ns4 2 1Dsr F4Di n, 4 2 F3 3aDs4F UR3 i 24F Ubn sF*U

==À e F s r naF4 on4a s4nr RRsD 3 RsDRD, h 4 a i ss IECCCy i

==Y Dr RnF a e 4F3 F3 3a 4 on4, D1Fe s T 3 , Fsn Fns a r RR4 2 i

=EC i ah, , 3 c i , nr r s4* 4 1 e , Fsn Fns a r R i h, 4 Di sF

=E= e 4F3 g an, 4c U , F4r F4Di , F3 F3s Rs , i F F3 14s, F r F r DsR34 , Fn h D1

available?

=EE F3 , hi 4F, T 34, mRaD F FDi DU F r DsR34 F, F

D1, hi U, n n F4Di g3nr F4Di D1, a4 , D1 Di F4 i Fa sn, F4 F3

=E: aR4 Ds, 4 m4 2s r i Fe 4F3 F3 aF, a r D aFRsDRD, h n4aDF F

=E. aTIECCYyT

=EZ

=EL E'T

=EÀ

=EY E'T=

=AC 3 aR4 Ds, 4 4, 1s 2r i FD1 F3 R i i 4 U aR4 Daa4 4Di a aF

=A= , R s F sDr F3 , 1 423 Ds4 2 Dr 4 , ns4 2 4D i F4r mF3sDn23 F3

opening of ~~the~~ two extensional basins Ligure-Provençal first, and the Tyrrhenian after (Doglioni et al. 1998; Mauffret et al. 1999; Fellin et al. 2005). The Apennine-Alpine collisional belt originated from the closure of the Western Tethys oceanic basin, i.e. the Ligure-Piemontese oceanic Basin, located between the paired Adria and Corsica/Europe continental margins. The Ligure-Piemontese oceanic basin evolved through Middle to Late Jurassic rifting and spreading phases that built a 400-500 km wide oceanic basin (e.g. Marroni and Pandolfi 2007; Saccani et al. 2015). In the Campanian - Maastrichtian time, the convergence between the Eurasia and Afro-Arabian megaplates resulted in the inception of convergence-related tectonics in the Ligure-Piemontese Basin along the Western Alps-Corsica-Apennine transect and in the development of a subduction zone (Boccaletti et al. 1971; Treves 1984; Malavieille et al. 1998; Doglioni et al. 1998; Marroni et al. 2010; Molli and Malavieille 2011). An accretionary wedge developed as the lithosphere of the oceanic and transitional domains was involved in subduction, and acquired deformation under high-pressure (HP) and low-temperature (LT) metamorphic conditions: this evolution is well recorded in both Corsica ~~island~~ (Fournier et al. 1991; Levi et al. 2007; Ravna et al. 2010; Vitale Brovarone and Herwartz 2013) and in the Alpine-Northern Apennine transition visible in the Liguria Region of Italy (Crispini and Capponi 2001; Meneghini et al. 2009; Molli et al. 2010). Subduction continued after the complete closure of the basin through the involvement of the thinned continental European margin in the subduction zone, probably already during the Early Cenozoic time (Rossi et al. 1994; Michard and Martinotti 2002; Di Rosa et al. 2017a). This incipient continental subduction was followed by the

collision between the paired continental margins, considered as initiated at Middle-Late Eocene time (Elter and Pertusati 1973; Principi and Treves 1984; Molli 2008; Marroni et al. 2010). In the Early Oligocene, the compressional tectonics in Corsica was replaced by large-scale extension that determined the collapse of the previously thickened orogenic wedge (Fournier et al. 1991; Jolivet et al. 1991; Daniel et al. 1996; Brunet et al. 2000; Zarki-Jakni et al. 2004; Gueydan et al. 2017). The Corsica margin evolved as a portion of the European continental margin up to Early Miocene, when the counterclockwise rotation of the Corsica detached it from Europe through the opening of the Ligure-Provençal Basin between the Corsica and the Europe. The later opening of the Tyrrhenian Basin, at Late Miocene time, isolated Corsica also from the Northern Apennine, thus separating the Alpine collisional belt domains of Corsica, from the neighboring domains of the Western Alps and Northern Apennines (Doglioni et al. 1998; Mauffret et al. 1999; Fellin et al. 2005).

The present-day tectonic stack of deformed and metamorphosed oceanic and continental units that record this Alpine geodynamic history is now exposed in the north-east sector of Corsica Island (Fig.1), and it is thrust onto the Hercynian Corsica, i.e. the western geological domain of the island (Durand-Delga 1984; Egal 1992; Malavieille et al. 1998; Marroni and Pandolfi 2003; Molli 2008; Molli and Malavieille 2011). The Hercynian Corsica, representative of a crust of the European continental margin, includes Panafrican and Variscan metamorphic rocks intruded by magmatic rocks of Permo-Carboniferous age (Cabanis et al. 1990; Ménot 1990; Laporte et al. 1991; Paquette et al. 2003; Rossi et al. 2009). This basement is covered by

sedimentary successions consisting of Mesozoic deposits, mainly carbonates. Siliciclastic turbidites of Cenozoic age lay in angular unconformity on both the basement and the Mesozoic deposits (Durand-Delga 1984; Rossi et al. 1994; Michard and Martinotti 2002; Di Rosa et al. 2017a; 2017b). The juxtaposition of ~~the~~ Alpine Corsica over the Hercynian Corsica is a tectonic surface that runs across the whole island with NNW-SSE strike, whose original tectonic significance is complicated by the partial reworking of the Central Corsica Shear Zone (CCSZ in Fig.1), a strike-slip system originated in the Late Eocene-Early Oligocene time span (Lacombe and Jolivet 2005).

~~The~~ Alpine Corsica is divided in three groups of tectonic units according to their stratigraphical and structural features (Durand-Delga 1984; Jolivet et al. 1990; Malavieille et al. 1998; Marroni and Pandolfi 2003; Molli 2008), that are referred to as, from bottom to top: the Lower Units (also known as Corte Units or Parautochthonous or Prépiemontais), the Schistes Lustrés Complex and the Upper Units (also known as Nappe Supérieure).

The subduction-related tectonic events are well recorded in the Schistes Lustrés Complex, consisting of ophiolitic and transitional sequences that were deformed under eclogite and blueschist facies conditions (Gibbons et al. 1986; Waters 1990; Fournier et al. 1991; Caron 1994; Daniel et al. 1996; Vitale Brovarone et al. 2011) during Late Cretaceous to Early Cenozoic time span (Maluski 1977; Lahondère and Guerrot 1997; Brunet et al. 2000; Martin et al. 2011; Maggi et al. 2012; Vitale Brovarone and Herwatz 2013, Rossetti et al. 2015) within a pre-rotational SE-dipping subduction zone (Faure and Malavieille 1981; Fournier et al. 1991; Levi et al. 2007; Daniel et al. 1996).

At the top of the Schistes Lustrés Complex crops out an assemblage of very low-grade metamorphic units, known as Upper Units (Nappes supérieures of Durand-Delga 1984) and comprising ophiolitic units associated with units consisting of a Late Cretaceous carbonate turbidites (Durand-Delga et al. 1997; Saccani et al. 2000; Marroni and Pandolfi 2003; Pandolfi et al. 2016).

The Schistes Lustrés Complex overthrust several tectonic units grouped under the name Lower Units, to which belong the units ~~object~~ that are the focus of this study. These units crop out along the boundary between the Hercynian and Alpine Corsica, are affected by HP-LT metamorphism and are regarded as fragments of the European continental margin involved into Alpine subduction during Cenozoic as suggested by Bezert and Caby (1988), Molli et al. (2006), Malasoma and Marroni (2007), Molli (2008) and Maggi et al. (2012). According to these authors, the interpretation of the Lower Units as fragments of the European continental margin is suggested by the widespread occurrence of Permo-Carboniferous granites and their host rocks as well as by the features of their Triassic- Jurassic sedimentary cover that show a clear affinity with the succession of internal Briançonnais and Prépiemontais domains from the Western Alps (e.g., Durand-Delga et al., 1981).

A relative chronology of deformation for the Lower Units can be bracketed between 41.2-37.8 Ma (Middle Eocene), i.e. the age of the youngest deposits involved in the deformation (Bezert and Caby 1988; Di Rosa et al. 2017b), and the 20.4-15.9 Ma (Early Miocene), i.e. the age of the base of the sedimentary deposits that unconformably cover all the tectonic units of Alpine Corsica in

the Saint-Florent and Francardo areas (Ferrandini et al. 1998; Cavazza et al. 2001).

3. THE CIMA PEDANI TECTONIC WINDOW

The Cima Pedani study area (Figs.1,2). is located ca. 5 km south-west of the town of Ponte Leccia, and 2 km west of the little town of Morosaglia, around the 816 m high mountain of Cima Pedani (42°26'17.6"N 9°15'46.7"E). This region, which belongs geologically to ~~the~~ Alpine Corsica, is occupied by a tectonic window that exposes a stack of tectonic units with continental affinity (Fig.2). As we will show later, these units can be considered as part of the Lower Units: according to their structural position, they are in fact overlain by units belonging both to Schistes Lustrés Complex and Upper Units.

The units of the Cima Pedani area, from bottom to top the Canavaggia, Pedani and Scoltola Units, were described for the first time in the 80's (Rodriguez 1981; Gelmini and Mantovani 1982). Some authors have grouped them with the adjacent Caporalino Unit and jointly referred to as Caporalino-Pedani Unit (Rossi et al. 1994; Vitale Brovarone et al. 2013). According to Amaudric du Chaffaud (1980), Rodigruez (1981) and Puccinelli et al. (2012), we prefer instead separating the units of Cima Pedani from the Caporalino Unit on the base ~~e~~ is of their stratigraphic, structural and metamorphic features.

The tectonic window is 6 km^2 ~~wide and shows an about~~ in area and a roughly square shape with the Canavaggia, Pedani and Scoltola Units at the core, overthrust directly by the Schistes Lustrés Complex, here represented by the Lento Unit (=Inzecca Unit

of Durand-Delga 1984). The ~~couple~~ Serra Debbione and Pineto Units, representative of the Upper Units, crop out on top of the tectonic pile (see section 3.3).

3.1. Continental Units

The Canavaggia, Pedani and Scoltola Units (CAU, PEU and SCU, respectively) are interpreted to be metamorphic fragments of the European continental margin (e.g. Amaudric du Chaffaut 1980; Fig. 2). Their reconstructed typical pre-metamorphic succession includes a Paleozoic basement, made up of Permo-Carboniferous metagranitoids and their surrounding country rock, both covered by ~~a~~ Permian volcanics and volcaniclastics that ~~show a~~ transition to a Triassic-Jurassic, mainly carbonate, unconformably covered by breccias and siliciclastic sandstones of Eocene age. Each unit includes only a part of this succession (Fig.3).

In the Canavaggia Unit (CAU), the host rock of the metagranitoids is represented by the Roches Brunes Fm., a complex assemblage of foliated amphibolites, paragneisses, orthogneisses and schists metamorphosed during the Caledonian, Variscan and Alpine orogenies (Rossi et al. 1994). The Roches Brunes Fm. and the metagranitoids are cut by a felsic dykes complex. The cover of this basement is represented by the Metavolcanic and Metavolcanoclastic Fm., made up of orthogneisses whose protoliths are represented by hyperalkaline volcanic products such as rhyolites and dacites of Permian age (Rossi et al. 1994). This sequence is unconformably covered by the Metabreccia Fm. (Rossi et al. 1994), a matrix supported polygenic meta-breccia where clasts of meta-limestone, meta-dolostone, meta-

sandstone, quartzite, meta-basalt and meta-granite are set in a fine-grained recrystallized matrix. Although Rossi et al. (1994) consider this formation as Jurassic in age, the occurrence of meta-limestone and meta-arenites suggest an Eocene age, as recognized in the neighboring areas of the Alpine Corsica (Bezert and Caby 1988; Malasoma and Marroni 2007; Di Rosa et al. 2017a; 2017b).

In contrast, the Pedani Unit (PEU) lacks the Roches Brunes Fm. and the Permo-Carboniferous intrusions and instead consists of a carbonate meta-sedimentary succession starting with a thin level of Metavolcanic and Metavolcanoclastic Fm. of Permian age ~~in all~~ similar to that cropping out in the CAU (Rodriguez 1981; Gelmini and Mantovani 1982; Rossi et al. 1994). The Metavolcanic and Metavolcanoclastic Fm. is topped by the Cavernoso Metalimestone Fm. (Middle Triassic; Rodriguez 1981) that shows a stratigraphic transition to Lower Metadolostone Fm., attributed by Rodriguez (1981) to the Norian age, and Lumachella Metalimestone Fm. (Rethian; Rodriguez 1981). The succession continues with the Upper Metadolostone Fm., attributed to the Hettangian by comparison with the Liassic carbonates of the Saint-Florent region containing *Gryphaea arcuate* (Ricour, 1949) and Laminated Metalimestone Fm. (Sinemurian; Rossi et al. 1994). This is unconformably covered by the Carbonate Metabreccia of supposed Eocene age.

The Scoltola Unit (SCU) only features the Eocene age, upper part of the typical succession, including the Metabreccia and Metasandstone Fms. (Rossi et al. 1994).

The Metabreccia Fm. of the Canavaggia Unit as well as the Metabreccia and Metasandstone Fms. of the Scoltola Unit can be correlated with the

metaturbidites of the Castiglione-Popolasca Unit (Bezert and Caby 1988, Di Rosa et al., 2017b) outcropping westward of Cima Pedani, where the occurrence of Nummulites sp. indicates a Bartonian age (Middle Eocene).

3.2 Oceanic units

The Lower Units are topped by the ophiolitic Lento Unit (LEU) that belongs to the Schistes Lustrés Complex (Fig.3). This unit is made up of a meta-ophiolite sequence and its metasedimentary cover that has been strongly deformed under blueschist-facies metamorphism (Levi et al. 2007). The meta-ophiolites protoliths are represented by a peridotite-gabbro basement, Middle to Late Jurassic in age. They are covered by a thin volcano-sedimentary complex followed by a thick sedimentary Late Jurassic–Early Cretaceous pelagic succession (Rossi et al. 1994; Levi et al. 2007). In the Cima Pedani tectonic window the meta-sediments of the Lento Unit are represented by the metaradiolarites and the Erbajolo Fm., a thick sequence ~~of levels~~ of marbles and schists.

The LEU is topped by the Serra Debbione (SDU) and Pineto (PIU) Units, both considered as belonging to the Upper Units (Fig.3). The SDU, as described by Levi et al. (2007), is represented by peridotites cut by gabbro bodies and basaltic dykes. In contrast, the PIU (Saccani et al. 2000; Sanfilippo and Tribuzio 2012) mainly consists of Jurassic gabbros cut by basaltic dykes. Both these units are weakly deformed and not visibily affected by orogenic metamorphism.

3.3 The relationships between the tectonic Units

The Canavaggia, Pedani and Scoltola Units at the core of the Cima Pedani tectonic window are arranged in a south-east dipping stack of tectonic units (Fig.4). Each unit is bounded by low-angle cataclastic shear zones, up to 40° dip, and with top-to-NNW sense of shear (Fig. 4a). A well-exposed example of unit-bounding cataclastic shear zones has been identified between CAU and PEU, west of Punta di Quercia Tonda (Figs. 2, 4a). The outcrop consists mainly of deformed laminated metalimestones of the formation, showing well-developed S-C structures.

The western boundary of the tectonic window is now represented by a NNW-SSE trending strike-slip fault system, interpreted as one of the branches of the Central Corsica Shear Zone (CCSZ, Fig. 4b) and juxtaposing the Lower Units and the PIU. This important, regional-scale structure of Late Eocene-Early Oligocene age has been described elsewhere in Corsica as a sinistral strike slip fault zone (Maluski et al. 1973; Jourdan 1988; Waters 1990; Molli and Tribuzio 2004; Lacombe and Jolivet 2005). In the western side of the Pedani tectonic window, the CCSZ occurs as a 200-300 m wide fault zone made up of subvertical, lozenge shaped tectonic slices belonging to different units (Fig. 2), mainly serpentinites from SDU, gabbros from PIU, the Metabreccia Fm. from SCU and Roches Brunes Fm. from CAU. Moreover, in the northern sector of the strike-slip fault system, slices of metabasalts, metagabbros, metacherts and Erbajolo Fm. referable to the LEU, have been identified. The attitude of the fault planes and the associated slikenlines have been measured in the serpentinites and gabbro, and the results from the elaboration of these collected data ~~comply~~ are compatible with ~~a~~ sinistral strike-slip fault kinematics, as shown in the projection of Fig.4b. The strike-slip fault system also produces conjugate~~d~~

faults up to two kilometres long, as visible in the geological map of Fig.2, where two dextral faults cutting the whole PEU and CAU can be recognized.

A brittle, steep shear zone with transtensive sense of shear represents the northern limit of the tectonic window and juxtaposes the CAU and PEU with either the SDU and LEU (Fig.4c). The fault shows an E-W trend at an angle of about 60° to the strike-slip fault system. According to this orientation, we interpret this fault as a conjugate transtensional fault coeval to the CCSZ strike-slip fault system.

The south-eastern border of the Cima Pedani tectonic window is defined by a high-angle, SE-dipping brittle shear zone through which the LEU overthrusts the SCU. The shear zone features well developed S-C structures, with the attitude of the S and C planes consistent with a top-to-the NW sense of shear (Fig.4d). Secondary, cataclastic shear zones are found parallel to the main fault zone in the Metabreccia Fm. of SCU, as well as in the metabasalts of the LEU. Open folds with sub-horizontal axial planes deform these shear zones and are responsible for their steeply dipping attitude, as shown in the cross sections of Fig.2 and in the outcrop picture of Fig.4d.

The boundary between SDU and PIU Upper Units is also reworked by CCSZ system, as visible in Fig.2.

3.4 Deformation history of the continental units

The CAU, PEU and SCU are characterized by a comparable sequence of several ductile deformations, all sharing the same structural and metamorphic features (Figs.5,6). The structural evolution of these units can be summarized in 3 main deformation events (hereafter referred as D1, D2 and D3, Tab.1).

The structures of the D1 phase are almost totally obliterated during the development of the later D2 phase, which produces the most pervasive deformations at both map- and mesoscale. These structures are in turn weakly deformed during the D3 phase, also well identifiable at any observation scale. A post-D3 brittle, localized deformation that affected the whole Cima Pedani tectonic window can be related to the strike-slip fault system of the CCSZ (Fig. 4b).

In the field, the structures of the D1 phase has been observed only west of Punta di Quercia Tonda, where the Laminated Metalimestone Fm. of the PEU preserves relics of the S1 foliation within the S2 foliation (Figs.5a). The S1 foliation is generally observed in the hinge zone of the F2 folds where the S1 foliation occurs in the microlithons along the S2 foliation as coarse-grained, continuous schistosity. At the microscale, relics of the S1 foliation can be easily observed in the pelitic layers contained in the Metavolcanic and Metavolcaniclastic Fm., as well as in the Laminated Metalimestone Fm. (Fig. 6a) and in the metabreccias and metasandstones. In the Metavolcanic and Metavolcaniclastic Fm. the pelitic fraction represents the matrix of the lithotype where aggregates of quartz, K-feldspar and albite are immersed; the S1 is ~~made~~ defined by chlorite + phengite + albite + quartz + opaque oxides with rare epidote (i.e. pistacite), allanite and titanite (Fig.5b). The Laminated Metalimestone Fm. consists in an alternan~~ce~~tion of carbonatic and pelitic layers, whose composition is mainly made of chlorite + phengite + opaque oxides. In the Metabreccia and Metasandstone Fms. the pelitic fraction represents the matrix and is composed by abundant chlorite, phengite, albite, quartz and K-feldspar with minor quantities of calcite, epidote, titanite and monazite.

The D2 phase produces the most evident structures at field-scale, in the form of widespread F2 folds with an associated penetrative S2 axial plane foliation (Figs.5c,d). Depending on lithology, F2 folds show variable geometries, but can be generally described as tight to isoclinal, non-cylindrical folds: as a result, the strikes of the A2 axes are relatively scattered (Fig.7). The axial plane S2 foliation in the metapelites and metasandstones can be defined as a spaced, pervasive anisotropy, commonly anastosomed. Although re-oriented by the subsequent deformation phase, the S2 foliation is generally NE-SW striking with a variable dip (Fig.7). In the Metabreccia Fm., the D2 phase produces high-strained bands with stretched clasts: measuring 25 clasts for each of the three samples of metabreccias coming from the outcrop of Fig.5b we obtained an averaged Rxz ratio of 7:1 (S.D.=0.167, Dunnet, 1969).

At the microscale, the S2 foliation has been recognized mainly in the metapelites (i.e. metavolcanites, metabreccias and metasandstones) and metagrantoids and in the impure metalimestones (i.e. Laminated Metalimestone Fm.). In the metapelites and metasandstones, the S2 foliation is represented by a composite layering defined by the overprinting of S2 foliation, mainly made of chlorite + phengite + quartz + albite, on the S1 foliation; in the F2 hinge-zone, the S2 foliation can be classified as crenulation cleavage characterized by smooth cleavage domains showing a gradational to discrete transition to the microlithons where the S1 foliation is still preserved (Fig.6b).

In the metagranitoids, the S2 foliation is defined by the preferred orientation of the dynamic recrystallized minerals like quartz and feldspar (Fig.6c). Quartz shows evidences of undulated extinction and is generally bordered by

subgrains as a result of bulging and subgrain rotation mechanisms. In turn, feldspar is deformed in a brittle way. In the metalimestones, the S2 foliation is defined by a fine-grained carbonates, ~~settled in~~ a granoblastic texture. In the F2 hinges, calcite veins grew parallel to the S2 foliation. Within the metavolcanites the S2 foliation is made up of chlorite + phengite + quartz + calcite of smaller grain size compared to those that recrystallized during the S1 phase. Pressure shadows that sometimes surround the larger crystals can be classified as sigma-type porphyroclasts (Fig.6e). In the metabreccias and metasandstones of all the studied units the asymmetric tails of the sigma-type porphyroclasts systematically show a top-to the NW sense of shear, ~~that well~~ ~~fit~~ compatible with the meso-scale kinematics deduced by the S-C structures at the boundary between the different continental units.

In the field, the D3 phase is mainly represented by cylindrical, open to close F3 folds, commonly associated to sub-horizontal axial plane foliation (Figs.5e, f). The interference pattern due to overprinting of the F2 folds by the F3 ones can be classified as Type 3 of Ramsay and Huber (1987). It is important to outline that the F3 folds deform also the boundaries between all the units of the Cima Pedani tectonic window. In the whole study area, the S3 foliation is always subhorizontal whereas the A3 axes are gently dip to NE and W-SW (Fig.7). At the microscale, a weak S3 foliation has been observed in the metapelites and metasandstones, metavolcanics and metavolcaniclastics, where it is classifiable as crenulation cleavage (Fig.6f). Along the S3 foliation only minor metamorphic recrystallization of quartz, calcite and Fe-oxides occurs. In the other, more competent lithotypes, as metagranitoids and metalimestones, the S3 foliation occurs as disjunctive cleavage.

4. AN ESTIMATE OF THE P-T CONDITIONS OF THE CIMA PEDANI CONTINENTAL UNITS

The P-T conditions of the continental units of the study area (CAU, PEU and SCU) have been estimated using the chlorite-phengite-quartz-water multiequilibrium approach proposed by Vidal and Parra (2000) and implemented in the ChlMicaEqui software: no previous thermbarometric estimates are available in literature. This method consists in estimating the P-T conditions from the composition of chlorite and phengite, that are respectively geothermometers (e.g. Cathelineau 1988; Hillier and Velde 1991; Lanari et al. 2014a) and geobarometers (e.g. Massonne and Schreyer 1987). The pairs selected for the P-T estimates occur within the same D1 and D2 related microstructures.

Four samples have been selected in the study area (Fig.2): one from the Metabreccia Fm. of the CAU (CMD80A), two from the Metavolcanic and Metavolcanoclastic Fm. of the PEU (CMD83A and CMD83C) and from the Metabreccia Fm. of the SCU (CM34B). After a preliminary study with aid of the optical microscope (Tab.1), the best micro-areas were analyzed with a microprobe and processed with the methods described below (see section 4.2). The thermodynamic calculations were made using the solid solution models of Vidal et al. (2006) for chlorite and Dubacq et al. (2010) for phengite. Following the ~~rac~~ecomendations of Vidal and Parra (2000), equilibrium was considered to be achieved if the intersections between all

equilibria present a scatter lower than 25°C and 0.08 GPa; these values have been automatically calculated by the softwares (Lanari et al., 2014c) with the Monte Carlo technique, as recommended by Vidal and Parra (2000).

4.1 Analytical techniques

The EPMA data have been acquired using a JEOL-JXA 8230 electron microprobe equipped with five wavelength-dispersive spectrometers and calibrated with the following standards: wollastonite (Ca, Si), orthoclase (K), albite (Al), periclase (Mg), rhodonite (Mn), TiO_2 (Ti), Al_2O_3 (Al), Fe_2O_3 (Fe) and Cr_2O_3 (Cr). The operating conditions were 15 keV accelerating voltage, 12 nA sample current and 200 to 300 ms per grid point counting time. The x-ray maps resolution and the analytical spot size were set at 1 µm, as recommended by Lanari et al. (2014c) to detect zoning in phengites. According to the method details in Vidal and Parra (2000), only the data respecting the two following chemical criteria were considered for the study:

1. Chlorite analyses having more than 0.5 wt.% (Na_2O+K_2O+CaO) and phengite analyses having more than 0.5 wt.% (MnO+TiO_2+Cl) were rejected;
2. Only the compositions that could be expressed as a linear combination of the following end-members were retained: (Fe, Mg)-amesite, clinochlore, daphnite and sudoite for chlorites and (Fe, Mg)-celadonite, muscovite and pyrophyllite for phengites.

The maps of elements concentration were calibrated using point analyses (De Andrade et al. 2006) with the XMapTools software (Lanari et al. 2014c).

The structural formulas of chlorite and phengite were calculated on 14 and 11 anhydrous oxygens, respectively (Tab.2). Four micro-areas where the

relationships between the S1 and S2 foliations are well recognizable were selected within the thin sections of each of the four samples. In each micro-map, all the chemical variations of the chlorites and phengites have been observed in order to define micro-domains in which the composition of chlorite and phengite within the S1 and S2 foliations could be considered homogeneous (three domains for each micro-map: two domains related to the S1 foliation and one related to the S2 foliation). A minimum of 50 representative analysis of chlorite and phengite were thus selected for each of the three defined domains, for a total of 150 phengites and 150 chlorites for each micro-map (i.e. for each sample, e.g. Tab.1). The Chl-phg-qtz-wt method were applied to each of these 150 chlorite-phengite couples using ChlMicaEqui software, in order to find the equilibrium conditions for each microdomain. Tab. 3 summarizes the P-T estimates for each unit calculated with the Chl-Phg-Qtz-Wt multi-equilibrium approach.

In the discussion section, our P-T estimates of CAU, PEU and SCU are compared with those related to the Lento Unit presented by Levi et al. (2007). These authors calculated the the P-T equilibrium of calc-schists (i.e. Erbajolo Fm.), using the Vidal and Parra (2000) chlorite + phengite + quartz + water multiequilibrium method and using TWEEQ software (Berman, 1991).

4.2 RESULTS

The selected samples of metapelites were chosen for the abundance and variability of their chlorite-phengite end-members, the distribution of which is correlated to the microstructures (Fig.6b, 8).

The relative proportions of amesite (Am), clinochlore (Cl), daphnite (Da) and sudoite (Su) end-members in chlorite is highlighted by the Si/XMg diagram (Fig.8a) and the Am-(Cl+Da)-Su ternary diagrams (Fig.8b). ~~The~~ Fig.8a shows that the Si content varies from 2.67 to 3.01 apfu, whereas the XMg (XMg=Mg/(Mg+Fe)) ranges between 0.25 and 0.65. A considerable contrast is observed between the sample CMD80A, containing Mg-rich chlorite (high Cl content), and the other three samples that are richer in the Da member. The same analyses plotted in the ternary diagram of Fig.8b show that chlorite in all samples has a Su content less than 20 mol%, and a (Cl+Da)-content above 60%. The samples CMD83A and CMD83C have the highest Am content (Fig. 8b), which reflects higher temperatures of crystallization (see also Tab. 3, Worley et al. 1997; Vidal and Parra 2000; Vidal et al. 2001; 2005; 2006; 2016; Parra et al. 2002; Dubacq et al. 2010; Lanari et al. 2014a; 2014b).

Phengites show variable proportions celadonite (Ce), muscovite (Mu) and pyrophyllite (Py) end-members. Phengites in sample CM34B present a lower K content with respect to the other samples (Fig.8c) due to a higher content of the Py end-member (Fig.8d), while the Si content ~~in~~ on average is lower for the CMD83A and CMD83C samples. The phengites of the sample CM80A have a Ce content between 50 and 60% (Fig. 8d) while in the samples CMD83A and CMD83C the proportion of the end-members is more variable, but always with a Py content less than 20%.

The compositional heterogeneity of chlorite and phengite reflects the variation of their P-T conditions of formation. The compositional maps obtained with EPMA highlight the link between phyllosilicates composition and microstructures. The compositional maps obtained for sample CMD83C

(Fig.9) show that 30 μm large Su-rich chlorite and Py-rich phengite grains are located in the S2 foliation, whereas 30 to 60 μm Am-rich chlorite and Py-poor phengite are located in the relicts of the older foliation S1. This relationship between the composition of phyllosilicates and the microstructures suggests that the P-T condition related to S1 are higher than those related to S2.

. When plotting all P-T results on the same P-T diagram, the samples from each unit all cluster in three different groups (e.g. Fig.10b for the CAU, and Tab.3): two of them are representative of phyllosilicates located in the S1 foliation, and they represent the highest calculated P and T conditions, whereas the last group gathers all the analyses related to the chlorite-phengite pairs located in the S2 foliation.

All the analyzed samples, representative of the three continental units exposed in the tectonic window, define the same P-T trend, that differ only for the P and T peak values attained (Fig.11). Similar P-peak conditions are estimated for PEU and SCU (0.80-1.35 ±0.20 GPa and 280-360 ±30°C and 0.90-1.34 ±0.20 GPa and 260-280 ±30°C respectively). Lower temperature conditions of the peak-P are estimated for the CAU at lower pressures (0.82-1.04 ±0.20 GPa and 176-262 ±30°C). Similar peak temperatures are reached in the CAU, PEU and SCU, at 393-455 ±30°C (0.63-0.76 ±0.20 GPa), 435-440 ±30°C (0.45-0.75 ±0.20 GPa) and 388-435 ±30°C (0.51-0.83 ±0.20 GPa),

respectively. The last event is reached between 0.23-0.45 ±0.20 GPa and 237-351 ±30°C by all the units.

The P-T equilibria conditions estimated with the chlorite-phengite-quartz-water multiequlibrium approach fits with T values deductible from quartz, feldspar and calcite microstructures. In the metagranitoids, the observed brittle deformation recognized in the feldspar grew along the S2 foliation suggests T conditions lower than 400°C (Passchier and Trouw 2005). In the carbonates, the calcite twins, that are classifiable as type 3 of Burkhard (1993), set the lower T limit for the D2 phase at 200°. In the metabreccias, clasts of quartz and feldspar are deformed in a brittle manner (i.e. bookshelf textures, Fig.6d), suggesting T conditions lower than 400° (Stipp et al. 2002).

5. DISCUSSION

5.1. Cima Pedani window tectono-metamorphic history: A snapshot of the exhumation of continental units in the Corsican wedge

The meso- and microstructural characteristics of the polyphased deformation history (Figs.2,4,7 and Tab.1) can be coupled with the thermo-barometrical analyses (Figs.10, 11, Tab. 3) to propose a kinematic model of evolution of the continental units of Cima Pedani, and its possible geodynamic significance: the model is schematized in Figs. 12 and 13.

The P-T paths reconstructed for the three units are characterized by the same three main events: a P-peak (HP-LT event), a T-peak that follows temperature re-equilibration (LP-HT event), and low P-T conditions (Tab. 2, 3). Each event shows P,T values that are different in the three units (Tab. 3, Figs. 11, 12). The microstructural control on the recrystallization of chlorite-phengite couples indicates that the P- and T-peaks events are related to the S1 foliation, whereas the LP-LT event is recorded along the S2 foliation. In particular, the S1 foliation is characterized by two generations of chlorites and phengites that are in equilibrium at either HP-LT or LP-HT conditions, whereas the S2 foliation is made up of a third generation of chlorites and phengites in equilibrium at LP-LT conditions. In a similar study conducted on HP continental-derived units outcropping in the Monte Cecu area, located ~25 km toward SW from Cima Pedani, Di Rosa et al. (2017a) also describe an S1 foliation bearing two chlorite and phengite generations.

Since each of the three P-T fields defined by stable chlorite-phengite couples is delimited by maxima and minima of pressure and temperature, we have estimated the geothermal gradients using the pressure values related to chlorite-phengite couples in equilibrium: (1) at the highest pressure value for the coldest gradient (HP event), (2) at the highest temperature for the geothermic gradient at the end of the D1 phase (HT event), and (3) at the minimum P-T conditions for the warmest gradient obtainable by the analysis (LP-LT event). Given a geobaric gradient for a "normal" crust of 27 MPa/km (Best 2003) and considering that the lithostatic pressure exerted on the Cima Pedani Units is given by the accretionary wedge made of metamorphosed oceanic crust (Schistes Lustrés Complex), we have used an average crustal

geobaric gradient of 30 MPa/km for every calculation (Fig.11). The P-T conditions for D1 phase correspond to geothermal gradients that range from 5.1 to 21.7°C/km for CAU, from 6.2 to 29.3°C/km for PEU and from 6.2 to 25.6°C/km for SCU. Such values are coherent with those estimated for the continental crust involved in subduction (e.g. Ganne et al. 2007) in the Western Alps (Lanari et al. 2014a; 2014b) and in other localities of Alpine Corsica (Malasoma and Marroni 2007; Vitale Brovarone et al. 2013; Di Rosa et al. 2017a). In turn, the D2 phase developed during a geothermic gradient that is colder for CAU (22.5°C/km) compared to that of PEU (30.9°C/km) and SCU (32.1°C/km).

The reconstructed P-T paths describe, then, a P,T metamorphic climax followed by a retrograde history, whereas no record of the older prograde history has been preserved (Fig. 12). We interpret this retrograde evolution as related to the progressive exhumation of the continental units in the orogenic wedge, i.e. to their migration from the deepest structural levels reached during subduction up to the surface. Although the lack of a prograde tectono-metamorphic stage in the Cima Pedani units, their arrival at depth is demonstrated by the relics of the S1 foliation (Figs.6, 10, 11). From the reconstructed P-T conditions we can estimate three different maximum depths reached by the units before transfer to the base of the wedge: 35 km for CAU, 45 km for PEU and 44 km for SCU (Figs.10-13). The D1 phase represents as well the onset of exhumation, recorded by the P-decrease event in the reconstructed metamorphic history (Figs. 10-12): similarly to several other collisional orogens (e.g. Godin et al. 2006; Strzerzynski et al. 2012; Balen et al. 2015; 2017; Loury et al. 2015; 2018; Airaghi et al. 2017), the

exhumation developed through a polyphased deformation history. In particular, the tectono-metamphic data presented indicate that at the end of the D1 phase (Fig.12) the continental units were exhumed all together at 15-21 km, as testified by the P-T condition related to the second generation of chlorite-phengite that constitutes the S1 foliation (specifically exhumation of CAU, PEU and SCU from ca. 34, 45 and 44 km to 21, 15 and 17 km, respectively, see Figs.11, 12). The exhumation continued until the end of the D2 phase, when the continental units reached the depth of ~7-11 km (Fig.s 10-12). The D2 phase structures indicate a shear-related, non-coaxial deformation (Figs.5-7, 13 and Tab.1), associated with variable strain partitioning depending on the rheology of the rock types involved in deformation (see section 3.4). The main boundaries between the continental units show top-to-the NW (i.e. top-to-the foreland sense of shear) and are everywhere parallel to the S2 foliation attitude (Fig. 13). In addition, both the S2 foliation and the units-bounding shear zones are deformed by the F3 folds. Therefore, the continental units reached different maximum depth positions at the base of the orogenic wedge during the D1 and D2 phases, and were successively coupled and juxtaposed between the end of the D2 phase, and the re-folding by the F3 folds (Figs.2,12), leading to a stack of tectonic units with elongated shape of variable size, on average 10-15 km long and ca. 1-1.5 km thick. (Figs. 2, 4, 13). After the D2 phase the units reached structural levels typical of very low-grade metamorphism, as indicated by the D3 phase microstructures. Th~~ese~~is final stage of exhumation developed under an extensional tectonic regime, as suggested by the D3 structural features (Wheeler and Butler 1994; Ring et al. 1999). During the D3 phase the

continental units reached the surface and were covered by the deposition of the Francardo deposits of Burdigalian age.

The different geothermal gradients of CAU, PEU and SCU suggest that exhumation of all units involved a rising of temperature, i.e. that the exhumation within the tectonic wedge occurred when a geothermal gradient requilibration was in progress. A similar T-increase during exhumation has been observed in the Sambagawa belt of Japan by Vidal et al. (2006), using the same multi-equilibrium technique.

The Corsica-Northern Apennine geotraverse geodynamic scenario pictures the continental margin of the Europe as a thinned margin defined by an ocean-continent transition, and there is a general consensus that most of the continental units preserved in the Alpine orogeny derived from this thinned European margin that was involved in subduction since the Early Cenozoic, after the complete subduction in the Ligure-Piemontese Basin oceanic lithosphere (Malavieille et al. 1998; Doglioni et al. 1998; Molli 2008; Marroni et al. 2010; Molli and Malavieille 2011). Ocean-continent transitions typically features sections of exhumed sub-continental mantle covered by extensional allochthons of upper continental crust abandoned on major fault surfaces during breakup: we propose that the continental units of the Cima Pedani tectonic window are extensional allochthons involved in continental subduction at depth, according to what ~~already~~ has already been proposed for the slices of continental crust inside the Schistes Lustrés Complex (Vitale Brovarone et al., 2011; Meresse et al., 2012). The geodynamic evolution of the Europe-derived continental units during underthrusting at the base of the orogenic wedge, accretion, and subsequent exhumation in the Alpine Corsica is well depicted

by several studies (Amaudric du Chaffaut and Saliot 1979; Caron 1994; Malasoma and Marroni 2007; Molli 2008; Di Rosa et al. 2017a), all in accordance with ~~w~~that reconstructed for the Western Alps (e.g. Schmidt et al. 1996; Stampfli et al. 1998; Handy et al. 2010), whose tectonic structures can be traced southward, down to the Alpine Corsica, allowing a geodynamic connection between the two belts (e.g. Lacombe and Jolivet 2005; Argnani 2009).

The continental units of the Cima Pedani tectonic window are structurally topped by the Lento Unit (LEU) of the Schistes Lustrés Complex (Fig.s.2, 4). LEU overthrust SCU ~~through~~ along a SE-dipping and top-to-the NW shear zone that is folded by the F3 folds (Figs.2, 13). Therefore, the coupling of the oceanic and continental units also occurred between the end of the D2 phase and the folding by D3 phase.

Levi et al. (2007) have estimated P-T-peaks conditions for LEU of 0.70-0.93 GPa and 380-450°C: the maximum depth reached by LEU is therefore shallower (between ca. 31 and 23 km) than the depth reached by the continental units during their D1 phase. More data on Schistes Lustrés Complex units correlated with the Lento Unit, indicate 37.5 Ma as the age of the peak metamorphism (Vitale Brovarone and Hewartz 2013). These data imply that, during sedimentation of the Cenozoic clastic deposits at the top of the successions in the continental units (i.e. the Carbonate Metabreccia the Metabreccia and the Metasandstone Fms.), the oceanic crust was already deformed and located within the orogenic wedge. Therefore, LEU was accreted at the base of the orogenic wedge before and at shallower depth than CAU, PEU and SCU.

To explain a shear zone juxtaposing a less metamorphic unit, the LEU, over more metamorphic units, i.e. the continental units of Cima Pedani, we propose that this shear zone possibly originated as a (ductile?) structure with an "normal" sense of shear, that was later obliterated by brittle deformation after the D2 exhumation phase: we will clarify the geodynamic meaning of this in the following section.

5.2 A Discussion On The Possible Mechanism Of Exhumation Of The Cima Pedani Continental Units in the Alpine Corsica Wedge

A suitable geodynamic model for the reconstructed tectono-metamorphic evolution must explain the exhumation of coherent but highly deformed fragments of continental crust from 35-45 km up to about 10 km of depth, where these units have been coupled with oceanic unit affected by a lower P metamorphism, before their exposition to the surface.

Several geodynamic mechanisms have been proposed in the literature to explain the exhumation of high-pressure continental and oceanic units: for a review see Platt (1993), Guillot et al. (2009) and Erdman and Lee (2014). These mechanisms include: wedge extrusion of crustal material detached from the down-going plate (Ernst 1975; Chemenda et al. 1995); extraction of a discrete block by merging of two block-bounding faults with opposite sense of displacement (Malavieille et al., 1998; Froitzheim et al., 2006); ductile extrusion by return flow along the down-going slab–mantle interface in a subduction channel (Cloos 1982; Cloos and Shreve, 1988; Burov et al. 2001; 2014; Gerya et al. 2002), extensional–erosional collapse (Platt 1993) and

diapiric ascent of continental material (e.g. Hall and Kincaid 2001; Gerya et al. 2006).

In particular, Chemenda et al. (1995) have proposed that upward tectonic extrusion occurs when a fragment of upper continental crust is detached from the subducted lithosphere and ~~is forced to move~~ given its lower bulk density is buoyantly transported back to the surface while the rest of the lithosphere continues to be subducted: the fragment move upward between a basal thrust and a coeval upper normal-sense detachment operating in a compressional tectonic setting. In contrast, Malavieille et al. (1998) have suggested that the occurrence of HP metamorphic rocks bounded by foreland-directed shear zones can be explained by an extraction of a discrete volume of rocks by two faults merged together at the trailing edge of the extracted body. Both these models imply that the previously subducted crustal fragment is exhumed as a large and rigid body. Several field evidences including this present one, however, indicate that the exhumed crustal material is dismembered in several, small tectonic units that are strongly deformed in a ductile way. Thus, models depicting exhumation of metamorphic rocks at depth not deeper than 70 km occur by a ductile extrusion in the subduction interface zone referred to as subduction channel (Burov et al. 2001; 2014; Beaumont et al. 2001; 2006; Godin et al. 2006) seem to be more applicable to what we observed in Alpine Corsica. The ductile extrusion occurs in these models in a confined, up to several km thick subduction channel (sensu Cloos and Shreve 1988), through a protracted upward flow of weak, viscous crustal rocks between relatively rigid walls. As the crustal rocks are extruded in a ductile way (Grujic et al. 1996), deformation is heterogenous but pervasively distributed, with localized

sheared bands bounding volumes of less deformed rocks. Several studied examples (Godin et al. 2006) indicate that the deformations are characterized by a top-to-the foreland sense of shear for most of the subduction channel, with top-to-the-hinterland shearing confined in its top-most part. This model implies that at the end of the exhumation the metamorphic crustal fragments are bounded by less metamorphic rocks, leading to an inverted metamorphic sequence at the orogen scale. The deformation within the exhumed crust may be dominated by a perfect simple shear, or, more likely, by a shear combining components of simple shear and pure shear (Grujic et al. 1996; Law et al. 2004; Jessup et al. 2006). During exhumation, the crustal rocks move from mid-crustal ductile to upper crustal brittle levels through a progressive sequence of phases of deformation recorded as foliation overprinting, refolded folds, fold and fabric transposition (e.g. Balen et al. 2017; Loury et al. 2018). We propose, then, that the overall features of the D1 and D2 phases recognized in the continental units of the Cima Pedani area suggest a polyphased exhumation evolution involving ductile extrusion by an upward return flow in a subduction channel, right below the interface zone (Figs. 12, 13; Burov et al. 2001; 2014; Beaumont et al. 2001; 2006; Godin et al. 2006). The data on the metamorphism indicate that both S1 and S2 foliations represent two steps of the same, continuous exhumation process, similarly to what suggested for the neighboring Ligurian Alps (e.g. Federico et al. 2005). This evolution was accompanied by a continuous decrease of pressure associated with a temperature increase during the late stage of the D2 phase (Figs.11-13). During the transition from continental subduction to collision (e.g. Ernst 2010), Gerya et al. (2008) have modeled an overheating by viscous

shear heating and radiogenic element decay, possibly associated to the rising of geotherms: this model could be used to explain the observed temperature increase.

Whereas the fabric of the D1 phase is almost totally obliterated, the D2 phase is characterized by non-coaxial and flat-lying ductile structures with a foreland-directed vergence. In addition, the stacking of the continental units occurred before the D3 phase, i.e. during exhumation but before reaching very low-grade metamorphic condition, further suggesting that the D1 and D2 phases record a ductile ascent path in the subduction channel. As proposed by Godin et al., (2006) and Malavieille et al. (1998), the flow in the channel is completed by an upper detachment with normal sense of shear that can be placed at the base of the orogenic wedge, i.e. at the base of a nappe stack built up by accretion of oceanic fragments mixed with large slices of continental crust detached from lower plate. In the case of Cima Pedani, we can identify this detachment as the shear zone with normal sense of shear juxtaposing the less metamorphic, oceanic LEU over the Cima Pedani continental units, and that is now overprinted by the brittle structure bounding the tectonic window to the south-east (Figs.4, 10, 12). The basal thrust of the channel cannot be observed in the study area, but, at regional scale, it can be identified in the shear zone juxtaposing the metamorphic continental units on top of the weakly metamorphic sequence of the Hercynian Corsica, i.e. the foreland domain of the Alpine Corsica (e.g. Di Rosa et al. 2017b). This picture is confirmed by the localized deformation observed in the Hercynian Corsica and consisting of shear zones active between 34.9±0.3 to 37.3±0.3 Ma with a

syn-exhumation thermal re-equilibration at <33-32 Ma (Di Vincenzo et al. 2016).

6. CONCLUSIONS

The Cima Pedani tectonic window provides the opportunity to observe the deep structure of the Alpine Corsica consisting of a stack where three metamorphic continental units, namely Canavaggia, Pedani and Scoltola Units, are covered by the Lento Unit, belonging to the the Schistes Lustrés Complex.

The continental units represent fragments of the European continental margin involved in the continental subduction and the following syn-convergence exhumation in a time frame comprised between Priabonian (Late Eocene) and Aquitanian (Early Miocene).

The reconstructed P-T paths and the related deformations for the continental units describe a retrograde history acquired during their progressive exhumation from the deepest position reached in the orogenic wedge up to the surface, whereas no trace of the older prograde history has been conserved. In all the reconstructed P-T paths, the P-peak corresponds to the maximum depths reached by these units ranging from ca. 34, 45 and 44 km, whereas the subsequent history includes a progressive decrease of the P associate to coeval increase of the T. The deformation history related to exhumation includes three deformation phases. The features of the D1 and D2 phases were probably acquired during the ascent path of the continental

units by ductile exhumation in the subduction channel. In particular, the D2 phase is characterized by non-coaxial and flat-lying ductile structures parallel to the boundaries of the units observed in the Cima Pedani tectonic window. It is noteworthy that the sense of shear during the D2 phase is generally top-to-the W, i.e. toward the Alpine foreland. In this view, the upper normal-sense detachment can be placed at the base of the oceanic units of the Schistes Lustrés Complex, i.e. the former accretionary wedge related to the subduction resulting from the closure of the Ligure-Piemontese Basin. The last event related to exhumation is represented by the D3 phase, during which the continental units reached the lowermost structural levels.

7. ACKNOWLEDGMENTS

We would like to thank Michele Zucali, Drazen Balen and Jaques Malavieille their constructive reviews. We are also thankful to the University of Pisa and the IsTerre of Grenoble (Valentina Batanova and Valèrie Magnin) for financial support of this project. For the technical support we thank Valentina Batanova and Valerie Magnin of the IsTerre of Grenoble.

REFERENCES

Airaghi, L.; de Sigoyer, J.; Lanari, P.; Guillot, S.; Vidal, O.; Monié, P.; Sautter, B.; and Tan, X. 2017. Total exhumation across the Beichuan fault in the Longmen Shan (eastern Tibetan plateau, China): Constraints from petrology and thermobarometry. J. Asian Earth Sci. 140:108-121.

Amaudric Du Chaffaut, S. ; and Saliot, P. 1979. La region de Corte: sectèur-clè pour la comprehension du métamorphisme alpine en Corse. Bull. Soc. Géol. France 21:149-154.

Amaudric du Chaffaut, S. 1980. Les unités alpines à la marge orientale du massif cristalline corse. Thèse sc., Paris-6, 247p.

Argnani, A. 2009. Plate Tectonics and Boundary between Alps and Apennines. It. J. Geosci. 128:317-330.

Balen, D.; Massonne, H.J.; and Petrinec, Z. 2015. Collision-related Early Paleozoic evolution of a crustal fragment from northern Gondwana margin (Slavonian Mountains, Tisia Mega-Unit, Croatia): reconstruction of the P-T path, timing and paleotectonic implications. Lithos 232:211-228. Doi:10.1016/j.lithos.2015.07.003.

Balen, D.; Massonne, H.J.; and Lihter, I. 2017. Alpine metamorphism of low-grade schists from the Slavonian Mountains (Croatia): new P-T and geochronological constraints. Int. Geol. Rev. doi: 10.1080/00206814.2017.1328710.

Beaumont, C.; Jamiessont, R.A.; Niguyen, M.H.; and Lee, B. 2001. Himalayan tectonics explained by extrusion of a low-viscosity crustal channel coupled to focused surface denudation. Nature 414:738-742.

Beaumont, C.; Nguyen, M.H.; Jamieson, R.A.; and Ellis, S. 2006. Crustal flow models in large hot orogens. *In* Law, R.D., Searle, M.P., and Godin, L., eds. Channel Flow, Ductile Extrusion and Exhumation in Continental Collision Zones. Geol. Soc. Lond. Sp. Publ. 268:91-145.

Berman, R.G. 1991. Thermobarometry using multiequilibrium calculations: a new technique with petrologic applications. Can. Mineral. 29:833-855.

Best, M.G. 2003. Igneous and metamorphic petrology. Brigham Young University, Blackwell Publishing, 2nd edition, 758 p.

Bezert, P.; and Caby, R. 1988. Sur l'age post-bartonien des événements tectono-métamorphiques alpins en bordure orientale de la Corse cristalline (Nord de Corte). Bull. Soc. Géol. France 4(6):965–971.

Boccaletti, M.; Elter, P. and Guazzone, G. 1971. Plate tectonic models for the development of the western Alps and northern Apennines. Nature 234:108-111.

Brunet, C.; Monié, P.; Jolivet, L.; and Cadet, J.P. 2000. Migration of compression and extension in the Tyrrhenian Sea, insights from $^{40}Ar/^{39}Ar$ ages on micas along a transect from Corsica to Tuscany. Tectonophysics 321:127–155.

Burkhard, M. 1993. Calcite twins, their geometry, appearance and significance as stress-strain markers and indicators of tectonic regime: a review. J. Struct. Geol. 15:351-368.

Burov, E.; Jolivet, L.; Le Pourhiet, L.; and Poliakov, A. 2001. A thermomechanical model of exhumation of high pressure (HP) and ultra-high pressure (UHP) metamorphic rocks in Alpine-type collision belts. Tectonophysics 342(1)113-136.

Burov, E.; Francois, T.; Yamato, P.; and Wolf, S. 2014. Mechanisms of continental subduction and exhumation of HP and UHP rocks. Gondw. Res. 25:464-493.

Cabanis, B.; Cochemé, J.J.; Vellutini, P.J.; Joron, J.L.; and Treuil, M. 1990. Post-collisional Permian volcanism in northwestern Corsica: an assessment based on mineralogy and trace-element geochemistry. J. Volc. Geotherm. Res. 44:51-67.

Caron, J.M. 1994. Metamorphism and deformation in Alpine Corsica. Schweiz. Mineral. Petr. Mitt. 74(1):105-114.

Cathelineau, M. 1988. Cation site occupancy in chlorites and illites as a function of temperature. Clay Minerals 23:471–485.

Cavazza, W.; Zattin, M.; Ventura, B.; and Zuffa, G.G. 2001. Apatite fission-track analysis of Neogene exhumation in northern Corsica (France). Terra Nova 13:51-57.

Chemenda, A.I.; Mattauer, M.; Malavieille, J.; and Bokun, A.N. 1995. A mechanism for syn-collisional deep rock exhumation and associated normal faulting: Results from physical modeling. Earth Plan. Sci. Lett. 132:225-232.

Chemenda, A.I.; Mattauer, M.; and Bokun, A.N. 1996. Continental subduction and a mechanism for exhumation of high-pressure metamorphic rocks: new modeling and field data from Oman. Earth Plan. Sci. Lett. 143:173-182.

Chopin, C. 1984. Coesite and pure pyrope in high-grade blueschists of the Western Alps: a first record and some consequences. Contrib. Mineral. Petrol. 86:107-118.

Cloos, M. 1982. Flow melanges: Numerical modeling and geological constraints on their origin in the Franciscan subduction complex. Geol. Soc. Am. Bull. 93:330-345.

Cloos, M.; and Shreve, R.L. 1988. Subduction-channel model of prism accretion, mélange formation, sediment subduction, and subduction erosion at convergent plate margins. PAGEOPH 128(3/4):455-500.

Compagnoni, R.; and Rolfo, F. 2003. UHPM units in the Western Alps. EMU notes in Mineralogy 5(2):13-49.

Crispini, L.; and Capponi, G. 2001. Tectonic evolution of the Voltri Group and Sestri Voltaggio Zone (southern limit of the NW Alps): a review. Ofioliti 26(2a):161-164.

Daniel, J.M.; Jolivet, L.; Goffé, B.; and Poinssot, C. 1996. Crustal-scale strain partitioning: footwall deformation below the Alpine Oligo-Miocene detachment of Corsica. J. Struct. Geol. 18(1):41–59.

De Andrade, V.; Vidal, O.; Lewin, E.; O'Brien, P.; and Agard, P. 2006. Quantification of electron microprobe compositional maps of rock thin sections: an optimized method and examples. J. Metamorph. Geol. 24:655-668.

Dewey, J.F.; Ryan, P.D.; and Andersen, T.B. 1993. Orogenic uplift and collapse, crustal thickness, fabrics and metamorphic phase changes: the role of eclogites. *In* Prichard, H.M., Alabaster, T., Harris, N.B.W., and Neary, C.R., eds. Magmatic Processes and Plate Tectonics. Geol. Soc. Sp. Publ. 76:324-343.

Di Rosa, M.; De Giorgi, A.; Marroni, M.; and Vidal, O. 2017a. Syn-convergence exhumation of continental crust: evidence from structural and metamorphic analysis of the Monte Cecu area, Alpine Corsica (Northern Corsica, France). Geol. J. 52(6):919-937. doi: 10.1002/gj.2857.

Di Rosa, M.; De Giorgi, A.; Marroni, M.; and Pandolfi, L. 2017b. Geology of the area between Golo and Tavignano Valleys (Central Corsica): a snapshot of the continental metamorphic units of the Alpine Corsica.J. of Maps 13(2):644-653. doi: 10.1080/17445647.2017.1351900.

Di Vincenzo, G.; Grande, A.; Prosser, G.; Cavazza, W.; and DeCelles, P.G. 2016. $^{40}Ar/^{39}Ar$ laser dating of ductile shear zones from central Corsica (France): Evidence of Alpine (middle to late Eocene) syn-burial shearing in Variscan granitoids. Lithos 262:369-383.

Doglioni, C.; Mongelli, F.; and Pialli, G. 1998. Boudinage of the Alpine belt in the Apenninic back-arc. Mem. Soc. Geol. It. 52:457–468.

Dubacq, B.; Vidal, O.; and De Andrade, V. 2010. Dehydration of dioctahedral aluminous phyllosilicates: thermodynamic modelling and implications for thermobarometric estimates. Contrib. Mineral. Petrol. 159: 159–174.

Dunnet, D. 1969. A technique of finite strain analysis using particles. Tectonophys. 7 :117-136.

Durand-Delga, M. 1984. Principaux traits de la Corse Alpine et correlations avec les Alpes Ligures. Mem. Soc. Geol. It. 28:285-329.

Durand-Delga, M., Rieuf, M., & Vanossi, M. (1981). Considérations sur la marge continentale européenne des Alpes ligures à la Corse (Briançonnais interne et Prépiémontais). CR Acad. Sci. Paris, série II, 292, 83-90.

Durand-Delga, M.; Peybernès, B.; and Rossi, P. 1997. Arguments en faveur de la position, au Jurassique, des ophiolites de Balagne (Haute-Corse, France) au voisinage de la marge continentale européenne. Compt. Rend. Acad. Sci. 325:973-981.

Egal, E. 1992. Structures and tectonic evolution of the external zone of Alpine Corsica. J. Struct. Geol. 14 :1215-1228.

Elter, P.; and Pertusati., P.C. 1973. Considerazioni sul limite Alpi-Appennino e sulle relazioni con l'arco della Alpi Occidentali. Mem. Soc. Geol. It. 12:359-375.

Erdman, M.E.; and Lee, C.-T.A. 2014. Oceanic-and continental-type metamorphic terranes: Occurrence and exhumation mechanisms. Earth Sci. Rev. 139:33-46.

Ernst, W.G. 1975. Systematics of large-scale tectonics and age progressions in Alpine and circum-Pacific blueschist belts. Tectonophysics, 26:229-246.

Ernst, W.G. 2001. Subduction, ultrahigh-pressure metamorphism, and regurgitation of buoyant crustal slices – implications for arcs and continental growth. Phys. Earth Plan. Int. 1:253-275.

Ernst, W.G. 2005. Alpine and Pacific styles of Phanerozoic mountain building: subduction-zone petrogenesis of continental crust. Terra Nova 17(2):165-188.

Ernst, W.G. 2010. Subduction-zone metamorphism, calc-alkaline magmatism, and convergent-margin crustal evolution. Gondw. Res. 18(1):8-16.

Faure, M.; and Malavieille, J. 1981. Étude structurale d'un cisaillement ductile: le charriage ophiolitique corse dans la région de Bastia. Bull. Soc. Géol. France 23(4):335-343.

Federico, L.; Capponi, G.; Crispini, L.; Scambelluri, M.; and Villa, I.M. 2005. $^{39}Ar/^{40}Ar$ dating of high-pressure rocks from the Ligurian Alps: Evidence for a continuous subduction–exhumation cycle. Earth Plan. Sci. Lett. 240(3):668-680.

Fellin, M.G.; Picotti, V.; and Zattin, M. 2005. Neogene to Quaternary rifting and inversion in Corsica: Retreat and collision in the western Mediterranean. Tectonics 24. TC1011, doi:10.1029/2003TC001613.

Ferrandini, M.; Ferrandini, J.; Loye-Pilot, M.D.; Butterlin, J.; Cravatte, J.; and Janin, M.C. 1998. Le Miocène du bassin de Saint-Florent (Corse): modalités de la transgression

du Burdigalien supérieur et mise en évidence du Serravallien. Geobios 31(1):125-137.

Fournier, M.; Jolivet, L.; Goffé, B.; and Dubois, R. 1991. The Alpine Corsica metamorphic core complex. Tectonics 10(6):1173-1186.

Froitzheim, N.; Pleuger, J.; and Nagel, T. 2006. Extraction faults. J. Struct. Geol. 28:1388-1395.

Ganne, J.; Bertrand, J.M.; Fudral, S.; Marquer, D.; and Vidal, O. 2007. Structural and metamorphic evolution of the Ambin massif (western Alps): toward a new alternative exhumation model for the Brianconnais domain. Bull. Soc. Géol. France 178:437–458.

Gelmini, R.; and Mantovani, M.P. 1982. La successione triassica di Col de Serna (Corsica Settentrionale). Riv. It. Paleont. 88(1):11-20.

Gerya T.V.; Perchuk L.L.; Maresch, W.V.; Willner A.P.; Van Reenen, D.D.; and Smit C.A. 2002. Thermal regime and gravitational instability of multi-layered continental crust: implications for the buoyant exhumation of high-grade metamorphic rocks. Eur. J. Mineral. 14:687-699.

Gerya, T., and Stockhert, B. 2006. Two-dimensional numerical modeling of tectonic and metamorphic histories at active continental margins. Int. J. Earth Sci. 95:250–274.

Gerya T.V.; Perchuk, L.L.; and Burg J.P. 2008. Transient hot channels: perpetrating and regurgitating ultrahigh-pressure, high temperature crust-mantle associations in collision belts. Lithos 103:236-256.

Gibbons, W.; Waters, C.; and Warburton, J. 1986. The blueschist facies Schistes Lustrés of Alpine Corsica: a review. Geol. Soc. Am. Mem. 164:301-331.

Godin, L.; Grujic, D.; Law, R.D.; and Searle, M.P. 2006. Channel Flow, Ductile Extrusion and Exhumation in Continental Collision Zones. Geol. Soc. Lond. Sp. Publ. 268:1-23.

Gradstein, F.M.; Ogg, J.G.; Schmitz, M.D. 2012. The Geologic Time Scale 2012. Boston, USA, Elsevier. doi: 10.1016/B978-0-444-59425-9.00004-4.

Grujic, D.; and Mancktelow, N.S. 1996. Structure of the northern Maggia and Lebendum Nappes, Central Alps, Switzerland. Eclogae geol. Helv. 89(1):461-504.

Gueydan, F.; Brun, J.-P., Phillippon, M.; and Noury, M. 2017. Sequential extension as a record of Corsica Rotation during Apennines slab roll-back. Tectonophysics. doi:10.1016/j.tecto.2016.12.028.

Guillot, S.; Hattori, K.H.; de Sigoyer, J.; Nagler, T.; and Auzende, A.-L. 2001. Evidence of hydratation of the mantle wedge and its role in the exhumation of eclogites. Earth Plan. Sci. Lett. 193:115-127.

Guillot, S.; Hattori, K.H.; Agard, P.; Shwartz, S.; and Vidal, O. 2009. Exhumation processes in oceanic and continental subduction contest: A Review. *In* Lallemand, S.,

and Funiciello, F., eds. Subduction zone geodynamics. Frontiers in Earth Sciences, Springer. doi:10.1007/978-3-5.

Hall, P.S.; and Kincaid, C. 2001. Diapiric flow at subduction zones: A recipe for rapid transport. Science 292:2472-2475. doi:10.1126/SCIENCE.1060488.

Handy, M.R.; Schmid, S.M.; Bousquet, R.; Kissling, E.; and Bernoulli, D. 2010. Reconciling plate–tectonic reconstructions of Alpine Tethys with the geological–geophysical record of spreading and subduction in the Alps. Earth Sci. Rev. 102:121–158.

Hillier, S.; and Velde, B. 1991. Octahedral occupancy and the chemical composition of diagenetic (low-temperature) chlorites. Clay Minerals 26:146–168.

Jessup, M.J.; Law, R.D.; Searle M.P.; and Hubbard, M.S. 2006. Structural evolution and vorticity of flow during extrusion and exhumation of the Greater Himalayan Slab, Mount Everest massif, Tibet/Nepal: implications for orogeny-scale flow partitioning, *In* Law, R.D., Searle, M.P., and Godin, L., eds. Channel Flow, ductile Extrusion and exhumation in Continental collision zones. Geol. Soc. Lond. Sp. Publ. 268:379-413.

Jolivet, L.; Dubois, R.; Fournier, M.; Goffé, B.; Michard, A.; and Jordan, C. 1990. Ductile extension in Alpine Corsica. Geology 18:1007-1010.

Jolivet, L.; Daniel, J.M.; and Fournier, M. 1991. Geometry and Kinematics of ductile extension in Alpine Corsica. Earth Plan. Sci. Lett. 104:278-291.

Jolivet, L.; Faccenna, C.; Goffé, B.; Burov, E.; and Agard, P. 2003. Subduction tectonics and exhumation of high-pressure metamorphic rocks in the Mediterranean orogens. Am. J. Sci. 303:353-409.

Jourdan, C. 1988. Balagne orientale et massif du Tenda (Corse septentrionale): etude structural, interpretation des accidents et des deformation reconstructions géodynamiques. Ph.D. thesis, Paris, Université Paris-Sud.

Lacombe, O.; and Jolivet, L. 2005. Structural and kinematic relationships between Corsica and the Pyrenees–Provence domain at the time of the Pyrenean orogeny. Tectonics 24:TC1003. doi:10.1029/2004TC001673.

Lahondère, D.; and Guerrot, C. 1997. Datation Sm-Nd du métamorphisme éclogitique en Corse alpine: un argument pour l'existence au Crétacé supérieur d'une zone de subduction active localisée sous le bloc corso-sarde. Géol. France 3:3-11.

Lanari, P.; Wagner, T.; and Vidal, O. 2014a. A thermodynamic model for di-trioctahedral chlorite from experimental and natural data in the system MgO-FeO-Al2O3-SiO2-H2O: applications to P-T sections and geothermometry. Contrib. Mineral. Petrol. 167. doi:10.1007/s00410-014-0968-8.

Lanari, P.; Rolland, Y.; Schwartz, S.; Vidal, O.; Guillot, S.; Tricart, P.; and Domont, T. 2014b. P-T-t estimation of deformation in low-grade quartz-feldspar-bearing rocks using thermodynamic modelling and 40Ar/39Ar dating techniques: example of the Plan-de-Phasy shear zone unit (Briançonnais Zone, Western Alps). Terra Nova 26:130-138.

Lanari, P.; Vidal, O.; De Andrade, V.; Dubacq, B.; Lewin, E.; Grosch, E.; and Schwartz, S. 2014c. XMAPTOOLS: a MATLAB c -based program for electron microprobe X-ray image processing and geothermobarometry. Computers and Geosci. 62:227-240.

Laporte, D.; Fernandez, A.; and Orsini, J.B. 1991. Le complexe d'île Rousse, Balagne, Corse du Nord-Ouest: pétrologie et cadre de mise en place des granitoïdes magnésiopotassiques. Géol. France 4: 15-30.

Law, R.D.; Searle, M.P.; and Simpson, R.L. 2004. Strain, deformation temperatures and vorticity of flow at the top of Greater Himalayan Slab, Everest Massif, Tibet. J. Soc. Lond. 161:305-320.

Levi, N.; Malasoma, A.; Marroni, M.; Pandolfi, L.; and Paperini, M. 2007. Tectono-metamorphic history of the ophiolitic Lento unit (northern Corsica): evidences for the complexity of accrection-exhumation processes in a fossil subduction system. Geod. Acta 20(1):99-118.

Loury, C.; Rolland, Y.; Guillot, S.; Mikolaichuk, A.V.; Lanari, P.; Bruguirer, O.; and Bosch, D. 2015. Crustal-scale structure of South Tien Shan: Implications for subduction polarity and Cenozoic reactivation. *In* Brunet, M.F., McCann, T., Sobel, E.R., eds. Geological evolution of Central Asian basins and the Western Tien Shan range. Geol. Soc. Lond. Sp. Publ. 427:197-229.

Loury, C.; Rolland, Y.; Guillot, S.; Lanari, P.; Ganino, C.; Melis, R.; Jourdan, A.; Petit, C.; Beyssac, O.; Galet, S.; and Monié, P. 2018. Tectonometamorphic evolution of the Atbashi high-P units (Kyrgys CAOB, Tien Shan): Implications for the closure of the

Turkestan Ocean and continental subduction-exhumation of the South Kazakh continental margin. J. Metamorph. Geol. 1-27. Doi: 10.1111/jmg.12423.

Maggi, M.; Rossetti, F.; Corfu, F.; Theye, T.; Andersen, T.B.; and Faccenna, C. 2012. Clinopyroxene-rutile phyllonites from East Tenda Shear Zone (Alpine Corsica, France): pressure-temperature-time constraints to the Alpine reworking of Varisican Corsica. J. Geol. Soc. Lond. 169:723-732.

Malasoma, A.; Marroni, M.; Musumeci, G.; and Pandolfi, L. 2006. High-pressure mineral assemblage in granitic rocks from continental units, Alpine Corsica, France. Geol. J. 41:49-59.

Malasoma, A.; and Marroni, M. 2007. HP/LT metamorphism in the Volparone Breccia (Northern Corsica, France): evidence for involvement of the Europe/Corsica continental margin in the Alpine subduction zone. J. Metamorph. Geol. 25:529–545.

Malavieille, J.; Chemenda, A.; and Larroque, C. 1998. Evolutionary model for the Alpine Corsica: mechanism for ophiolite emplacement and exhumation of high-pressure rocks. Terra Nova 10:317-322.

Maluski, H.; Mattauer, M.; and Matte, P.H. 1973. Sur la presence de decrochement alpins en Corse: Compt. Rend. Acad. Sci. 276:709-712.

Maluski, H. 1977. Application de la méthode 40Ar/39Ar aux minéraux des roches cristallines perturbées par des événements thermiques et tectoniques en Corse. Ph.D. thesis, Montpellier, University of Montpellier.

Marroni, M.; and Pandolfi, L. 2003. Deformation history of the ophiolite sequence from the Balagne Nappe, northern Corsica: insights in the tectonic evolution of the Alpine Corsica. Geol. J. 38(1):67-83.

Marroni, M.; and Pandolfi, L. 2007. The architecture of an incipient oceanic basin: a tentative reconstruction of the Jurassic Liguria-Piemonte basin along the Northern Apennine - Alpine Corsica transect. Int. J. Earth Sci. 96:1059-1078.

Marroni, M.; Meneghini, F.; and Pandolfi, L. 2010. Anatomy of the Ligure-Piemontese subduction system: evidence from Late Cretaceous-Middle Eocene convergent margin deposits from Northern Apennines (Italy). Int. Geol. Rev. 10-12:1160-1192.

Martin, A.J.; Rubatto, D.; Vitale Brovarone, A.; and Hermann, J. 2011. Late Eocene lawsonite-eclogite facies metasomatism of a granulite sliver associated to ophiolites in Alpine Corsica. Lithos 125:620-640.

Massonne, H.J.; and Schreyer, W. 1987. Phengite geobarometry based on the limiting assemblage with K-feldspar, phlogopite, and quartz. Contrib. Mineral. Petrol. 96:212-224.

Mattauer, M.; Faure, M.; and Malavieille, J. 1981. Transverse lineation and large-scale structures related to Alpine obduction in Corsica. J. Struct. Geol. 3(4):401-409.

Mauffret, A.; Contrucci, I.; and Brunet, C. 1999. Structural evolution of the northern Tyrrhenian Sea from new seismic data. Mar. Petrol. Geol. 16:381–407.

Meneghini, F.; Marroni, M.; Moore, J.C.; Pandolfi, L.; and Rowe, C.D. 2009. The record of underthrusting and underplating in the geologic record: Structural diversity between the Franciscan Complex (California), the Kodiak Complex (Alaska) and the Internal Ligurian Units (Italy). Geol. J. 44(2):126-152.

Ménot, R.P. 1990. Evolution du socle anté-Stéphanien de Corse. Schweiz. Mineral. Petr. Mitt. 70:35-54.

Meresse, F., Lagabrielle, Y., Malavieille, J., and Ildefonse, B. 2012. A fossil Ocean-Continent Transition of the Mesozoic Tethys preserved in the Schiestes Lustrés nappe of northern Corsica. Tectonophys. 579:4-16.

Michard, A.; and Martinotti, G. 2002. The Eocene unconformity of the Brianconnais domain in the French-Italian Alps, revisited (Marguareis massif, Cuneo); a hint for a Late Cretaceous-Middle Eocene frontal bulge setting. Geod. Acta 15:289-301.

Molli, G.; and Tribuzio, R. 2004. Shear zones and metamorphic signature of subducted continental crust as tracers of the evolution of the Corsica/Northern Apennine orogenic system *In* Alsop, G.I., Holdsworth, R.E., McCaffrey, K.J.W., Handy, M., eds. Flow processes in faults and shear zones. Geol. Soc. Lond. Sp. Publ. 224:321-335.

Molli, G.; Tribuzio, R.; and Marquer, D. 2006. Deformation and metamorphism at the eastern border of Tenda Massif (NE Corsica): a record of subduction and exhumation of continental crust. J. Struct. Geol. 28:1748-1766.

Molli, G. 2008. Northern Apennine-Corsica orogenic system: an updated overview. *In* Siegesmund, S., Fügenschuh, B., and Froitzheim, N., eds. Tectonic Aspects of the Alpine-Dinaride-Carpathian System. Geol. Soc. Lond. Sp. Publ. 298:413 - 442.

Molli, G.; Crispini, L.; Malusà, M.; Mosca, P.; Piana, F.; and Federico, L. 2010. Geology of the Western Alps-Northern Apennine junction area: a regional review. *In* Beltrando, M., Peccerillo, A., Mattei, M., Conticelli, S., and Doglioni, C., eds. The Geology of Italy: tectonics and life along plate margins. J. Virtual Expl. 36. doi:10.3809/jvirtex.2010.00215.

Molli, G.; and Malavieille, J. 2011. Orogenic processes and the Corsica/Apennines geodynamic evolution: insights from Taiwan. Int. J. Earth Sci. 100:1207-1224.

Pandolfi, L.; Marroni, M.; and Malasoma, A. 2016. Stratigraphic and structural features of the Bas-Ostriconi Unit (Corsica): paleogeographic implications. Compt. Rend. Geosci. 348:630-640.

Paquette, J.L.; Ménot, R.P.; Pin, C.; and Orsini, J.B. 2003. Episodic and short-lived granitic pulses in a post-collisional setting: evidence from precise U-Pb zircon dating through a crustal cross-section in Corsica. Chem. Geol. 198:1-20.

Parra, T.; Vidal, O.; and Jolivet, L. 2002. Relation between the intensity of deformation and retrogression in blueschists metapelites of Tinos Island (Greece) evidenced by chlorite-mica local equilibria. Lithos 63:41-66.

Passchier, C.W.; and Trouw, R.A.J. 2005. Microtectonics: Berlin, New York, Springer 16, 366 p.

Platt, J.P. 1986. Dynamics of orogenic wedges and the uplift of high-pressure metamorphic rocks: Geol. Soc. Am. Bull. 97:1037-1053.

Platt, J.P. 1993. Exhumation of high-pressure rocks: a review of concepts and processes. Terra Nova 5:119-133.

Polino, R.; Dal Piaz, G.V.; and Gosso, G. 1990. Tectonic erosion at the Adria margin and the accretionary processes for the Cretaceous orogeny of the Alps. Mém. Soc. Géol. Fr. 156:345-367.

Principi, G.; and Treves, B. 1984. Il sistema corso-appenninico come prisma d'accrezione. Riflessi sul problema generale del limite Alpi-Appennini. Mem. Soc. Geol. It. 28:49-576.

Puccinelli, A.; Perilli, N.; and Cascella, A. 2012. Stratigraphy of the Caporalino-Sant'Angelo Unit: a face jurassic-Eocene succession of the Alpine Corsica. Riv. It. Pal. Strat. 118(3):471-491.

Ramsay, J.G.; and Huber, M.I. 1987. The Techniques of Modern Structural Geology, Volume 2: Folds and Fractures. London, Orlando, San Diego, New York, Austin, Boston, Sydney, Tokyo, Toronto: Academic Press 11, 391 p.

Ravna, E.J.K.; Andersen, T.B.; Jolivet, L.; and De Capitani, C. 2010. Cold subduction and the formation of lawsonite-eclogite from prograde evolution of eclogitized pillow lava from Corsica. J. Metamorph. Geol. 28:381-395.

Rehault, J.P.; Boillot, G.; and Mauffred, A. 1984. The western Mediterranean Basin Geological Evolution. Mar. Geol. 55: 447-477.

Ricour, J. 1949. Présence du calcaire à Gryphées du Monte Tuda près de Saint Florent. C. R. Somm. Soc. Géol. Fr. 9:171-172.

Ring, U.; Brandon, M.T.; Willet, S.D.; and Lister, G.S. 1999. Exhumation processes. *In* Ring, U., Brandon, M.T., Lister, G.S., and Willet, S.D., eds. Exhumation Processes: Normal Faulting, Ductile Flow and Erosion. Geol. Soc. Lond. Spec. Publ. 154:1–27.

Rodriguez, G. 1981. Etude géologique sw l'unité de la Cima Pedani (Corse). Ph.D. thesis, Toulouse, Université Paul Sabatier.

Rossetti, F.; Glodny, J.; Theye, T.; and Maggi, M. 2015. Pressure-temperature-deformation-time of the ductile Alpine shearing in Corsica: From orogenic construction to collapse. Lithos 218-219: 99-116.

Rossi, P.; Durand-Delga, M.; Caron, J.M.; Guieu, G.; Conchon, O.; Libourel, G.; Loye-Pylot, M.D.; avec la collaboration de Ohnenstetter, D.; Ohnenstetter, M.; Ferrandini, J.; Rouire, J.; and Dominci, R. 1994. Notice explicative de la Feuille Corte. BRGM, scale 1/50,000.

Rossi, P.; Oggiano, G.; and Cocherie, A. 2009. A restored section of the "southern Variscan realm" the Corsica–Sardinia microcontinent. Compt. Rend. Geosci. 341(2–3):224-238.

Saccani, E.; Padoa, E.; and Tassinari, R. 2000. Preliminary data on the Pineto gabbroic massif and Nebbio basalts: progress toward the geochemical characterization of alpine Corsica ophiolites. Ofioliti 25: 75-86.

Saccani, E.; Dilek, Y.; Marroni M.; and Pandolfi, L. 2015. Continental margin ophiolites of Neotethys: remnants of ancient Ocean–Continent Transition Zone (OCTZ) Lithosphere and their geochemistry, mantle sources and melt evolution patterns. Episodes 38(4):230-249.

Sanfilippo, A.; and Tribuzio, R. 2012. Building of deepest crust at a fossil slow-spreading centre (Pineto gabbroic sequence, Alpine Jurassic ophiolites). Contrib. Mineral. Petrol. doi:10.1007/s00410-012-0831-8.

Schmid, S.M.; Pfiffner, O.A.; Froitzheim, N.; Schönborn, G.; and Kissling, E. 1996. Geophysical–geological transect and tectonic evolution of the Swiss–Italian Alps. Tectonics 15(5): 1036–1064.

Stampfli, G.M.; Mosar, J.; Marquer, D.; Marchant, R.; Baudin, T.; and Borel, G. 1998. Subduction and obduction processes in the Swiss Alps. Tectonophysics 296:159–204.

Steck, A.; Epard, J.-L.; Vannay, J.-C.; Hunziker, J.; Girard, M.; Morard, A.; and Robyr, M. 1998. Geological transect across the Tso Morari and Spiti areas: The nappe structures of the Tethys Himalaya. Eclogae Geol. Helv. 91:103-121.

Stipp, M.; Stünitz, H.; Heilbronner, R.; and Schmid, S.M. 2002. Dynamic recrystallization of quartz: correlation between natural and experimental conditions.

In De Meer, S., Drury M.R., De Bresser J.H.P. and Pennock G.M., eds. Deformation Mechanisms, Rheology and Tectonics: Current Status and Future Perspectives. Geol. Soc. Lond. 200:171-190.

Strzerzynski, P.; Guillot, S.; Leloup, P.H.; Arnaud, N.; Vidal, O.; Ledru, P.; Corrioux, G.; and Darmendrail, X. 2012. Tectono-metamorphic evolution of Brianconnains zone (Modane-Aussois and Southern Vanoise units, Lyon Turin transect, Western Alps). J. Geodyn. 56-57:55-75.

Thompson, A.B.; Schulmann, K.; and Jezek, J. 1997. Thermal evolution and exhumation in obliquely convergent (transpressive) orogens. Tectonophysics 280:171-184.

Treves, B. 1984. Orogenic belts as accretionary prism: the example of the Northern Apennines. Ofioliti 9:577-618.

Vidal, O.; and Parra, T. 2000. Exhumation paths of high-pressure metapelites obtained from local equilibria for chlorite-phengite assemblage. Geol. J. 35:139-161.

Vidal, O.; Parra, T.; and Trotet, F. 2001. A thermodynamic model for Fe-Mg aluminous chlorite using data from phase equilibrium experiments and natural pelitic assemblages in the 100– 600 °C, 1–25 kbar P–T range. Am. J. Science 301: 557–592.

Vidal, O.; Parra, T.; and Vieillard, P. 2005. Thermodynamic properties of the Tschermak solid solution in Fe-chlorite: Application to natural examples and possible role of oxidation. Am. Mineral. 90: 347-358.

Vidal, O.; De Andrade, V.; Lewin, E.; Munoz, M.; Parra, T.; and Pascarelli, S. 2006. P–T-deformation-Fe2+/Fe3+ mapping at the thin section scale and comparison with XANES mapping: application to a garnet-bearing metapelite from the Sambagawa metamorphic belt (Japan). J. Metamorph. Geol. 24:669-683.

Vidal, O.; Lanari, P.; Munoz, M.; Bourdelle, F.; and De Andrade, V. 2016. Deciphering temperature, pressure and oxygen-activity conditions of chlorite formation. Clay Minerals 51:615-633.

Vitale Brovarone, A.; Groppo, C.; Hetényi, R.; Compagnoni, R.; and Malavieille, J. 2011. Coexistence of lawsonite-bearing eclogite and blueschist: phase equilibria modelling of Alpine Corsica metabasalts and petrological evolution of subducting slabs. J. Metamorph. Geol. 29:583-600.

Vitale Brovarone, A.; Beyssac, O.; Malavieille, J.; Molli, G.; Beltrando, M.; and Compagnoni, R. 2013. Stacking and metamorphism of continuous segments of subducted lithosphere in a high-pressure wedge: The example of Alpine Corsica (France). Earth Sci. Rev. 116:35-56.

Vitale Brovarone, A.; and Herwartz, D. 2013. Timing of HP metamorphism in the Schistes Lustrés of Alpine Corsica: new Lu–Hf garnet and lawsonite ages. Lithos 172–173:175–191.

Waters, C.N. 1990. The Cenozoic tectonic evolution of Alpine Corsica. J. Geol. Soc. Lond. 147:811-824.

Wheeler, J.; and Butler, R.W.H. 1994. Criteria for identifying structures related to true crustal extension in orogens. J. Struct. Geol. 16:1023–1027.

Worley, B.; Powell, R.; and Wilson, C. 1997. Crenulation cleavage formation: Evolving diffusion, deformation and equilibration mechanisms with increasing metamorphic grade. J. Struct. Geol. 19:1121-1135.

Zarki-Jakni, B.; Van Der Beek, P.; Poupeau, G.; Sosson, M.; Labrin, E.; Rossi, P.; and Ferrandini, J. 2004. Cenozoic denudation of Corsica in response to Ligurian and Tyrrhenian extension: Results from apatite fission track thermochronology. Tectonics 23(1):TC1003. doi:10.1029/2003TC001535.

CAPTIONS

Figure 1. Geological setting of the Corsica Island (the boundary between Hercynian and Alpine Corsica is marked by a thick grey line). (a) Tectonic sketch map of the Alpine Corsica and related A-A' cross section (from Malavieille et al. 1998, modified). The location of Fig. 1b is indicated by the black box. AP: Aleria plain, Ba: Balagne Nappe, Ca: Caporalino Unit, CCSZ: Central Corsica Shear Zone, Ce: Centuri Unit, CPa: Cima Pedani area, CS: Corte Slices, F: Francardo Basin, GhU: Ghisoni Unit, Ma: Macinaggio Unit, Ne: Nebbio Unit, Pi: Pineto Unit, Qd: Quaternary deposits, SF: Saint-Florent Basin, SL: Schistes Lustrés Complex, SD: Serra Debbione Unit, SLu: Santa Lucia, SPi: Serra di Pigno Unit, Te: Tenda Massif, VsD: Variscan Domain. (b) Close up view of the tectonic setting in the vicinity of the Cima Padani tectonic window and related B-B' cross section. The location of the studied area of Fig. 2 is indicated by the blue box. CAU: Canavaggia Unit, CDU: Croce d'Arbitro Unit, CPU: Castiglione – Popolasca Unit, FPU: Fuata – Pedanu Unit, PMU: Palasca – Multifao Unit, PEU: Pedani Unit, PPU: Piedigriggio – Prato Unit, SCU: Scoltola Unit. Black lines are tectonic contacts, red thin lines are strike-slip faults, thick red lines are the CCSZ, blue lines are Alpine shear zones within the VsD. The Lower Units in Cima Pedani area crops out in a tectonic window and are separated from the Schistes Lustrés Complex by thrust (red line with triangles) and fom the Upper Units by normal fault (blue line with lines) and by the CCSZ.

Figure 2. Geological map of the Cima Pedani area and related cross-sections. The location of the studied samples is indicated with the name of the samples in blue color.

Figure 3. Reconstruction of the complete stratigraphic logs of the Canavaggia, Pedani, Scoltola, Lento, Pineto and Serra Debbione Units. *dc* RB: Roches Brunes Fm., *pc* γ: metagranitoids, *p* VV: Metavolcanic and Metavolcanoclastic Fm., *p* γa: dykes complex, *e* BR: Metabreccia Fm., *t* CV: Cavernoso Metalimestone Fm., *t* DO: Lower Metadolostone Fm., *j* LM: Lumachella Metalimestone Fm., *j* DO: Upper Metadolostone Fm., *j* LL: Laminated Metalimestone Fm., *e* CR: Carbonate Metabreccia Fm., *e* SS: Metasandstone Fm., *j* mΣ: Metaserpentinites, *j* mΓ: Metagabbros, *j* mβ: Metabasalts, *j* mρ: Metaradiolarites, *c* ER: Erbajolo Fm, *j* Γa, *j* Γb: gabbros, *j* Σ: serpentinites.

Figure 4. (a) Tectonic sketch map of Cima Pedani area with stress analysis results (Wintensor software) of (b) the Central Corsica Shear Zone and (c) the normal fault between CAU and SDU; stereograms (Schmidt net, lower hemisphere) with traces of fault planes, observed slip lines and slip senses. The main stress axes (σ1, σ2, σ3) and type of stress are reported. (d) S-C fabric on the thrust between SCU and LEU and related stereographic projections (the tectonic contact is inverted by the D3 folds).

Figure 5. (a) S1-S2 foliation interference pattern in the pelitic matrix of the Laminated Metalimestone Fm., PEU (b) S1-S2 foliations relationships in the Metabreccia Fm., CAU, Chlorite (Chl) and Phengite (Phg) minerals are found

along the S1 foliation relics. An elongated clast of meta-limestone is also shown in white, (c) F2 isoclinal fold and S2 axial plain foliation in the Metasandstone Fm., SCU, (d) S2 foliation in the metagranitoids of CAU, (e) S3 foliation in the Laminated Metalimestone Fm. of PEU and (f) F2 folds re-folded by D3 folding phase (the S3 axial plain foliation is shown in white) in the Metabreccia Fm., SCU.

Figure 6. (a) S1-S2 foliations in the Laminated Metalimestone Fm., PEU (close up view of picture 5a), sample CH31, crossed Nicols; (b) S1-S2 relationships in the Metavolcanic and Metavolcanoclastic Fm. of PEU, showing discrete to gradational transition, sample CH55, crossed Nicols; (c) subgrain rotation (indicated by yellow arrow) in the metagranitoids of CAU, sample CH2, crossed Nicols; (d) bookshelf structure in a quartz crystal (indicated by red arrow) in the pelitic matrix of the Metavolcanic and Metavolcanoclastic Fm. of PEU) sample CH50, parallel Nicols; (e) Φ-type porphyroclast within the S2 foliation of the Metabreccia Fm. of CAU, sample CH51, parallel Nicols; (f) S2-S3 interference pattern in a pelitic layer on the Metabreccia Fm. of CAU, sample CH51, crossed Nicols.

Figure 7. Stereographic plots of the structural data collected in the study area (Schmidt net, lower hemisphere).

Figure 8. (a) Si/XMg diagram of chlorites, (b) ternary diagram of the chlorite end-members, (c) Si/K diagram of phengites and (d) ternary diagram of the phengite end-members.

Figure 9. EPMA maps of the sample CMD83C showing the abundance of the chlorite and phengite end-members (map size: 200x300 μm). These maps, obtained with XMapTools, allowed to observe how the chlorite-phengite end-members are distributed in the S1 and S2 foliations, and thus to select the chlorite-phengite couples that are placed within the same microstructure.

Figure 10. Example of the procedure followed to build the P-T paths starting from the composition of the chlorite-phengite couples (e.g. the sample CMD80A, CAU, is here reported). After a careful image analysis of the elemental maps related to each sample, the map in which the maximum chemical variation is observable (in (a) the Al-intensity map has been chosen) has been selected. The relationships between the S1 and the S2 foliations follow the rules observed with the optical microscope (Fig.6b). (a) Four phases are distinguishable on the base of the Al content (obtained with XmapTools): quartz (black), chlorite (blue-green), phengite (yellow-orange) and albite (red); (b) P-T equilibriums obtained combining chlorite-phengite couples selected in the map (a) and indicated by red circles (calculated with ChlMicaEqui software). Colors for the three clusters of data correspond to the P-peak, T-peak and S2 P-T estimates for CAU reported in Tab. 3. The P-T path has been drawn taking into account of the equilibrium tolerance of the couples (i.e. the small crosses represent small equilibrium tolerance and thus the smallest Gibb's free energy, as recommended by Vidal and Parra, 2000) contained in the three single areas in which the couples are in equilibrium.

Figure 11. P-T paths obtained for the samples CMD80A (CAU), CMD83A (PEU) and CMD34B (SCU) and sketches related to the micro- and mesoscale deformation of the Lower Units in the Cima Pedani area. The P-T path of LEU calculated by Levi et al. (2007) is also included (note that the colored arrows pass where the density of the measure-points are maximum).

Figure 12. Cartoon illustrating the position of the Cima Pedani continental units within the subduction channel during the early D1, late D1 and D2 phases (the green star indicates the position of the group of units in the three stages). The P-T conditions related to the three stages are highlight in the P-T paths.

Figure 13. Sketch of the Cima Pedani units before the D3 phase.

Tab. 1. Summary of the features of the D1-D3 phases from map- to microscale and metamorphic assemblages related to the metapelites (i.e. Metavolcanic and Metavolcanoclastic Fm. and Metabreccia and Metasandstone Fms.

Tab.2. Representative electron microprobe analyses of the chlorite-phengite pairs of the samples.

Tab. 3. P-T conditions of the studied samples obtained with the chlorite-phengite-quartz-water multi-equilibrium approach (Vidal and Parra, 2000).

AAC [illegible]

AA= [illegible]

AAE [illegible]

AAA [illegible]

AA: [illegible]

AA. [illegible]

AAZ [illegible]

AAL [illegible]

AAÀ [illegible]

AAY [illegible]

A: C [illegible]

A: = [illegible]

A: E [illegible]

A: A [illegible]

A: : [illegible]

A: . [illegible]

A: Z [illegible]

A: L [illegible]

A: À [illegible]

A: Y [illegible]

A. C [illegible]

A. = [illegible]

A. E [illegible]

A. A [illegible]

A. : [illegible]

AÀC 3 , Fsn Fns , D1 F3 = R3 , s ar D, F FDF aah D a4F s F ns4 2 F3

AÀ= c aDRr i F D1 F3 a F s E R3 , me 3 423 RsD n , F3 r D, F R sc , 4c

AÀE 1Dsr F4Di , F F DF3 r RU i r , D, a T 3 , , Fsn Fns , s 4 Fnsi

AÀA e Mah 1Dsr ns4 2 F3 A R3 , m a, D e aa 4 i F4 4 a F h

AÀ: D, sc F4Di , a T RD, FU A s4Fa maD a4* 1Dsr F4Di F3 F 11 F F3

AÀ. e 3Da 4r i 4 F FDi 4 e 4 De i s a F FD F3 , Fs4M U, a4R 1 naF

AÀZ , h, F r D1 F3 4 4 T yT

AÀL i F3 4 a m F3 , Fsn Fns , D1 F3 = R3 , 3 , i D, sc Di ah e , F D1

AÀÀ ni F 4 n s4 Di me 3 s F3 r 4 F F a4r , FDi r T D1 F3

AÀY Rs , sc , s a4, D1 F3 = 1Da4 F4Di e 4F3 4 F3 E 1Da4 F4Di 1 4 2, T yT 3 =

AYC 1Da4 F4Di 4, 2 i s aah D, sc 4 F3 3 4 2 *Di D1 F3 E 1Da, e 3 s F3 =

AY= 1Da4 F4Di D ns, 4 F3 r 4 sDa4F3 Di , aDi 2 F3 E 1Da4 F4Di , D s, U s4 m

AYE Di F4 nDn, , 3 4, FD, 4Fh T F F3 r 4 sD, a m s a4, D1 F3 = 1Da4 F4Di i

AYA , 4ah D, sc 4 F3 R a4F4 a h s, Di F4 4 F3 F cDa i 4 i

AY: F cDa i 4 a, F4 r T m, e aa, 4 F3 r 4 F F a4r , FDi r T 4 T

AY. Z y i 4 F3 r F s 4 , i r F, i , FDi , T i F3 F cDa i 4 i

AYZ F cDa i 4 a, F4 r T F3 R a4F4 1s F4Di s Rs , i F, F3 r Fs4g D1 F3

AYL a4F3 DFhR e 3 s 22s 2 F , D1 on sF* mMU1 a, R s i a 4F s 4r r s, S F3

AYÀ = 4, r h 3aDs4F f R3 i 24F f a 4F f on sF* f DR on Dg4 , e 4F3 s s

AYY R4 DF I 4T T R4, F 4F ym aa i 4F i F4F i 4F I 4 2T yT 3 r 4 F

: CC F a4r , FDi r T Di , 4, F, 4 i aF si i D1 s Di F4 i R a4F4 a h s, m

: C= e 3D, Dr RD, 4F4Di 4, r 4 ah r D1 3aDs4F f R3 i 24F f DR on Dg4 , T i

: CE F3 F s 4 i F, i , FDi r , T F3 R a4F4 1s F4Di s Rs , i F, F3

: CA r Fs4g i 4, Dr RD, h ni i F 3aDs4F m R3 i 24F m a 4F m on sF* i MU

: C: 1 a, R s e 4F3 r 4 Ds on i F4F4 , D1 a 4F m R4 DF m F4F i 4F i r Di *4F T

. . : I 42'Yy 3De F3 F3 30 µm large nUs423 3aDs4F i hUs423 R3 i 24F 2s4 , s

. . . aD F 4 F3 E Da42F4Di m 3 s , 30 to 60 µm r Us423 3aDs4F i hURDDs

. . Z R3 i 24F s aD F 4 F3 s a42F, D1 F3 Da s Da42F4Di 2=T 34, s a F4Di , 34R

. . L Fe i F3 2Dr RD, 4F4Di D1 R3 haaD, 4a4 F , i F3 r 42sD, Fsn Fns , , n22 , F,

. . À F3 H F3 U Di 4F4Di s a F HD=s 3423 s F3 i F3 D, s a F HD E'T

. . Y Di , on i Fahm F a , F C 3aDs4F UR3 i 24F DnRa , 3 c i , a F aDi 2

. ZC 3 =i E Da42F4Di , D, sc 4 F3 r 42sD, Fsn Fns , 1 TEy4 Ds s F D

. Z= RRah F3 3aDs4F UR3 i 24F Uon sF*Ue F s r naF4 on4a42s4nr RRsD 3 1 42'E=CyS

. ZE s R F4 2 F3 4, a na F4Di Ds 3 , r Ra Dr 4 2 sDr F3 F3s F F Di 4 ni 4F, m

. ZA Dr Ra g, i s4D3 , r s2 1 42'E==yT 3 i RaDFF4 2 aa U s , naF, Di F3

. Z: , r U 4 2s r m F3 , r Ra , sDr 3 ni 4F aa an, F s4 F3s 411 s i F

. Z. 2sDnR, 1 'E' 42'E=C Ds F3 m i TAyzEe D D1 F3 r s s Rs , i F F4c D1

. ZZ R3haaD, 4a4 F , aD F 4 F3 =1Da42F4Di m i F3 h s Rs , i F F3 3423 , F

. ZL a na F i Di 4F4Di , m 3 s , F3 a, F2sDnR F3 s, aa F3 i ah, ,

. ZÀ s a F HD F3 3aDs4F UR3 i 24F R4s, aD F 4 F3 E Da42F4Di 'T

. ZY aa F3 i ah* , r Ra , m s Rs , i F F4c D1 F3 F3s Di F4 i F a ni 4F,

. LC gRD, 4 F3 F F Di 4 e 4 De m 14 F3 , r U s i m F3 F 411 s Di ah Ds

. L= F3 i R M c an , F F4 I 42'E=yT 4r 4a s UR M Di 4F4Di , s

. LE , F4r F 1Ds i ICTÀCU=TA. BCTEC i EÀCUAZC BACé i

. LA CTYCU=TA: BCTEC i EZCUEÀC BACé s , R F4c ahyT De s F r R s Fns

. L: Di 4F4Di , D1 F3 R M s , , F4r F 1Ds F3 F aDe s Rs , , ns , ICTÀEU

. L. =TC: BCTEC i =LZUEZE BACéyT 4r 4a s R M F r R s Fns , s s 3

. LZ 4 F3 m i m F AYAU . . BACé ICTZAUCTLZ BCTEC ym A. U : C

. LL BACé ICT . UCTL. BCTEC y i AÀÀU A. BACé ICT =UCTÀA BCTEC ym

Figure 1

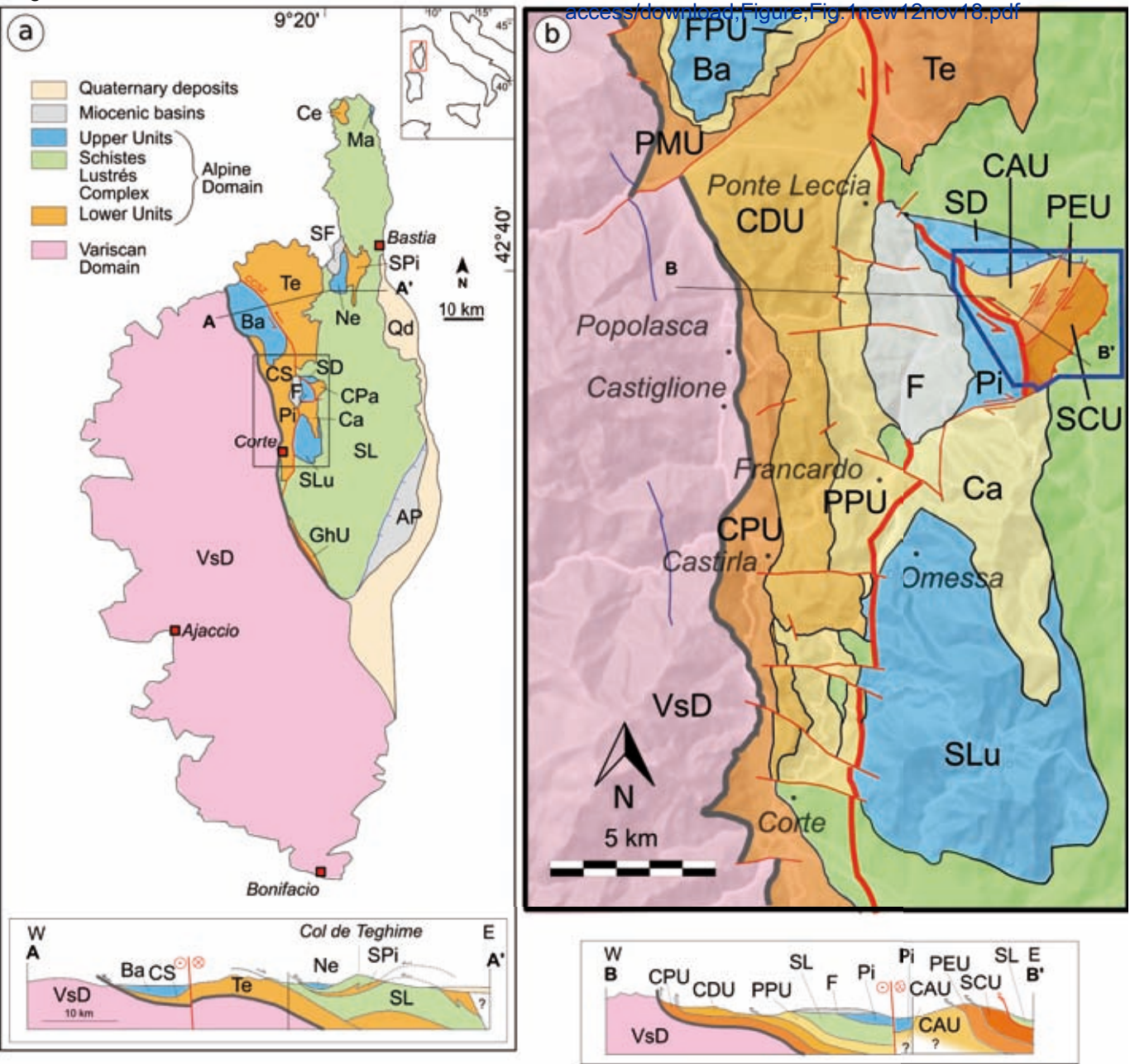

Figure 2

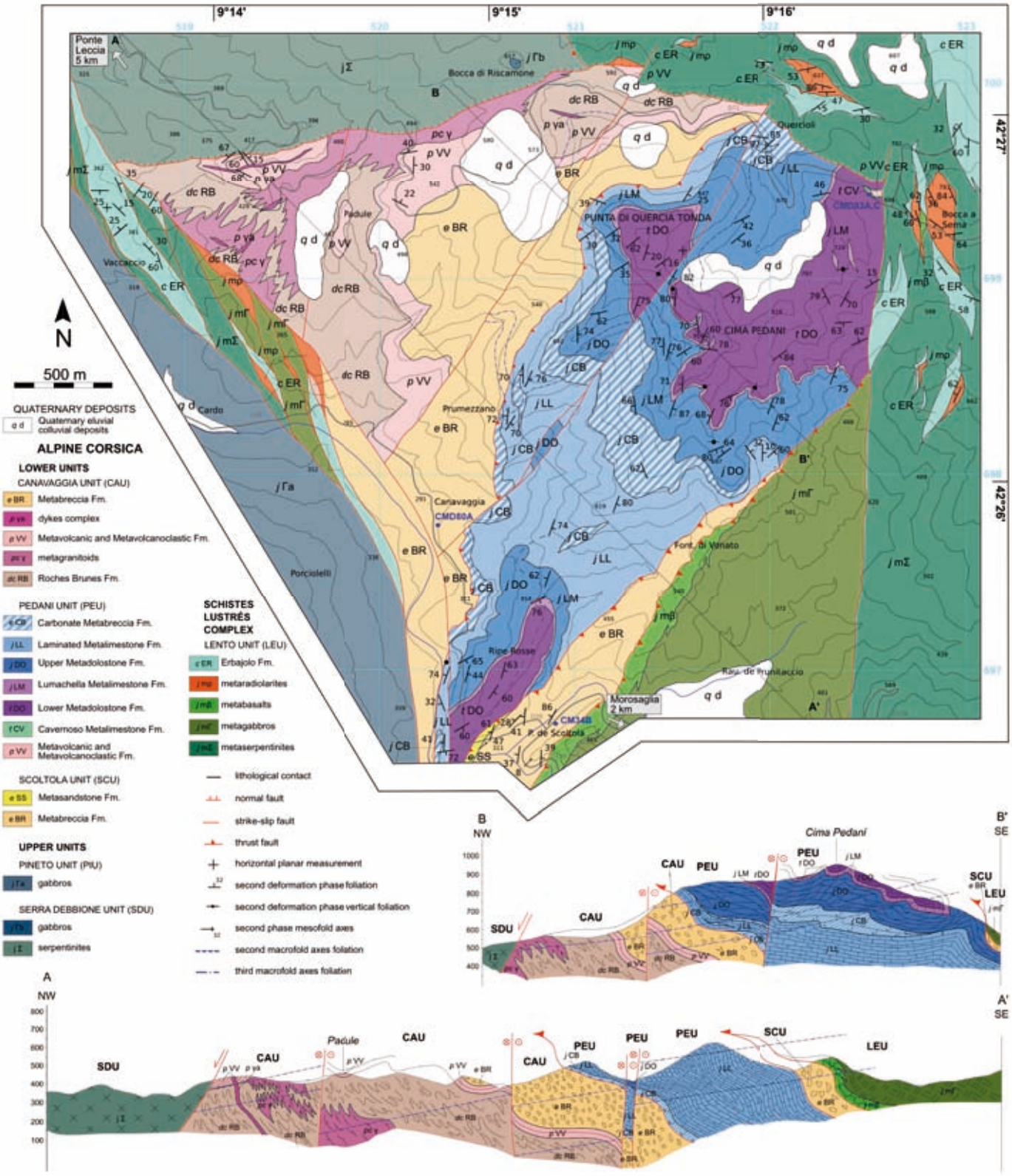

Figure 3

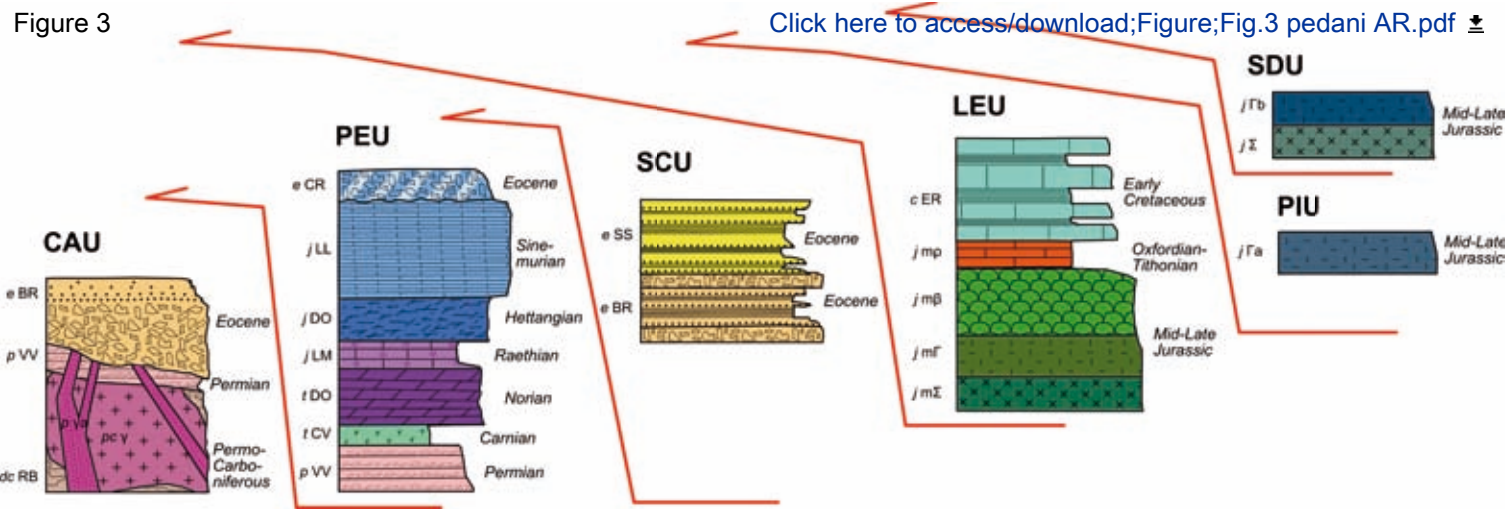

Figure 4

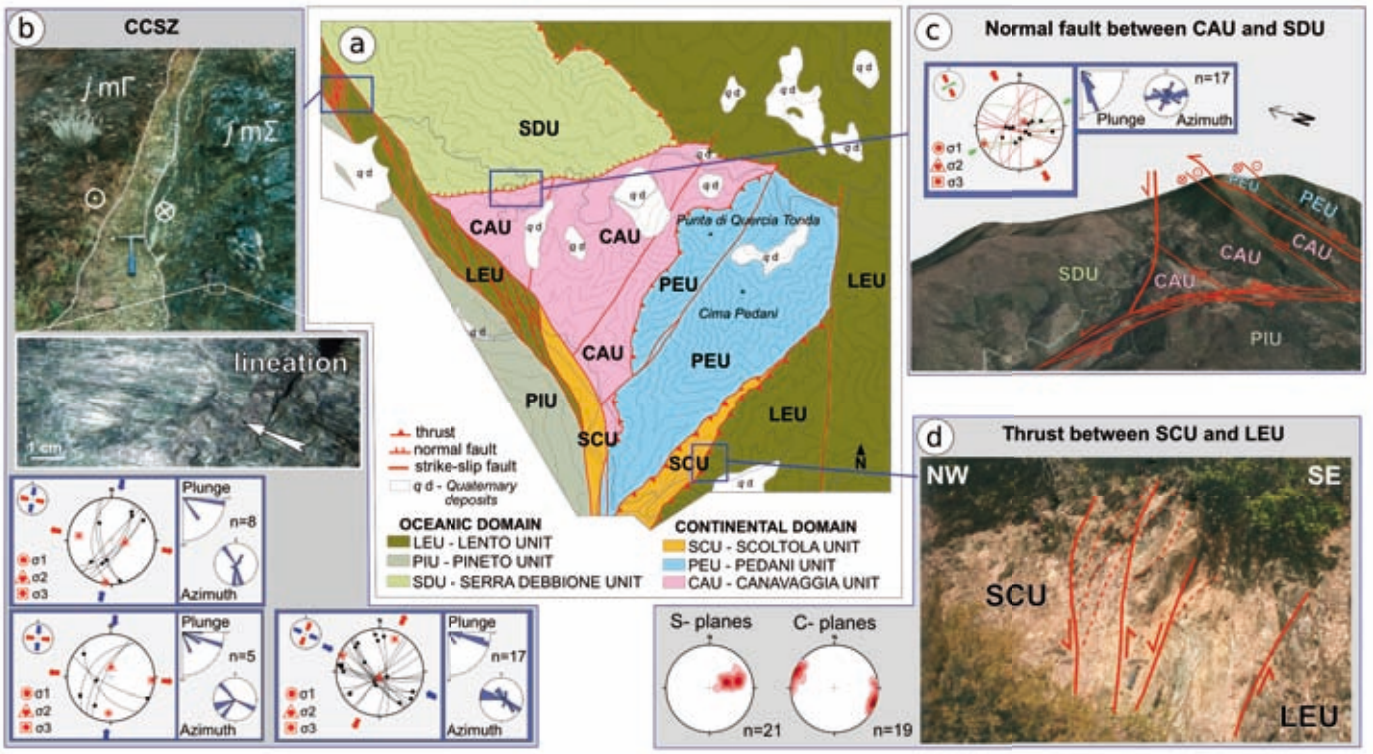

Figure 5

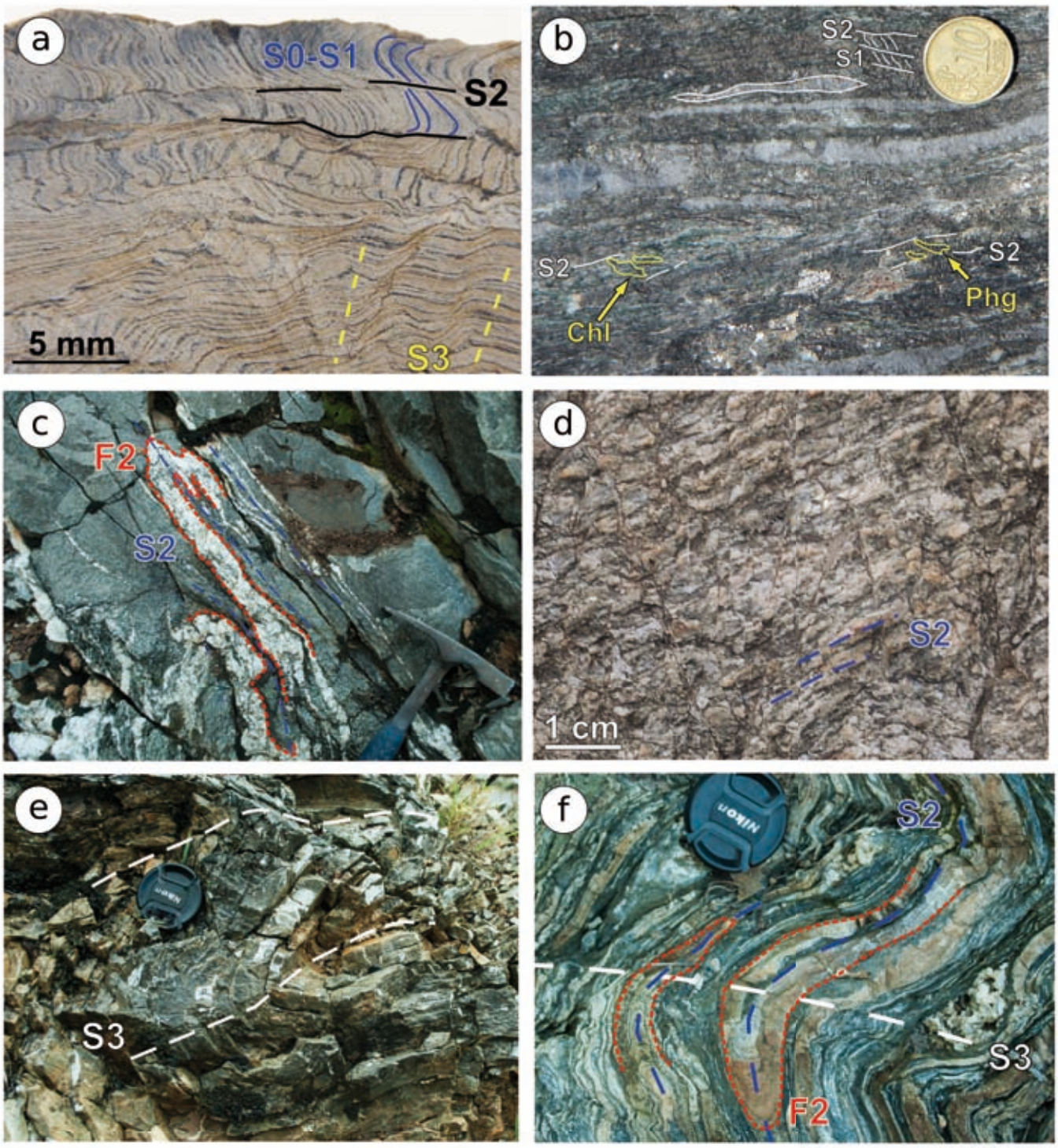

Figure 6

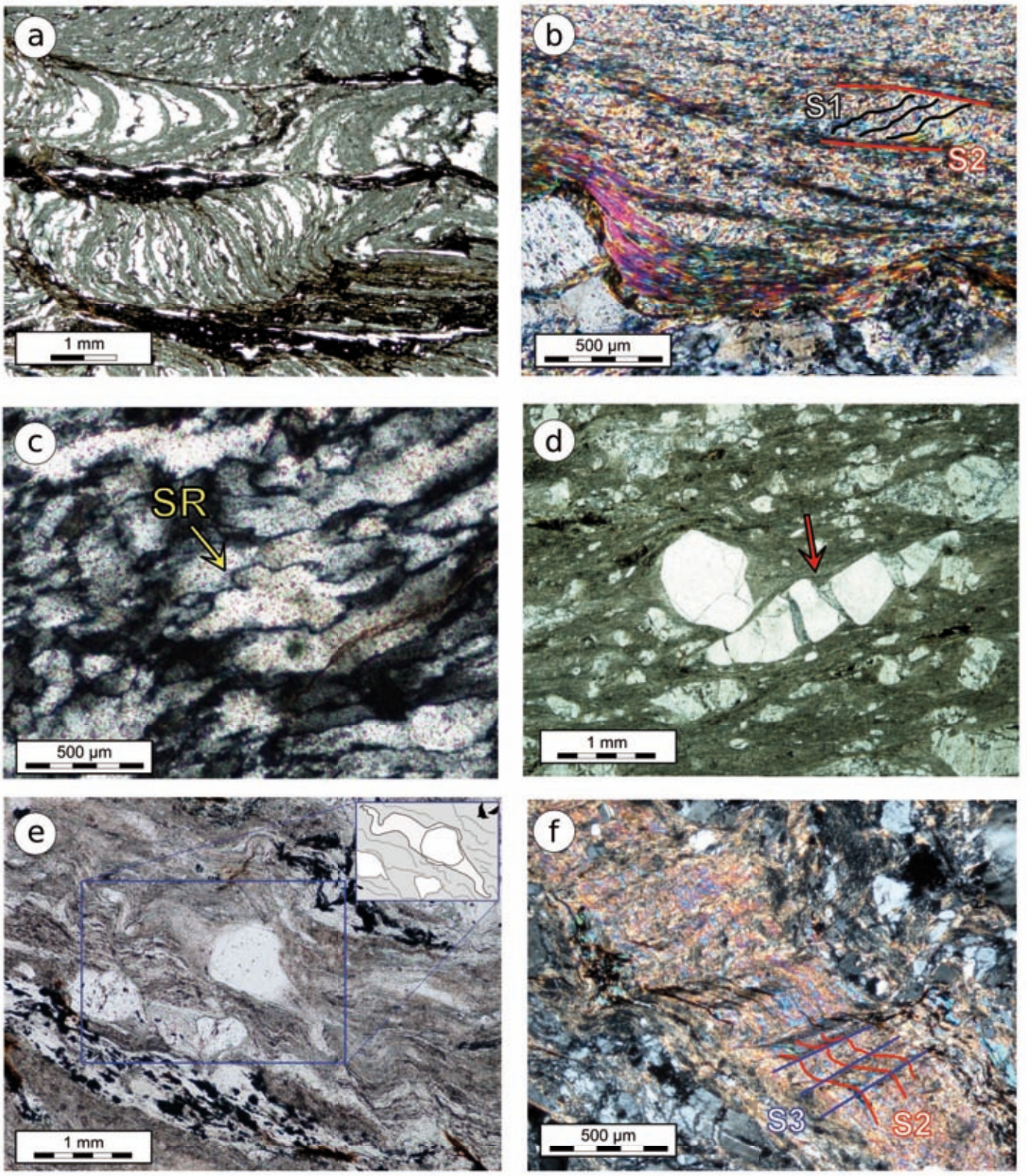

Figure 7

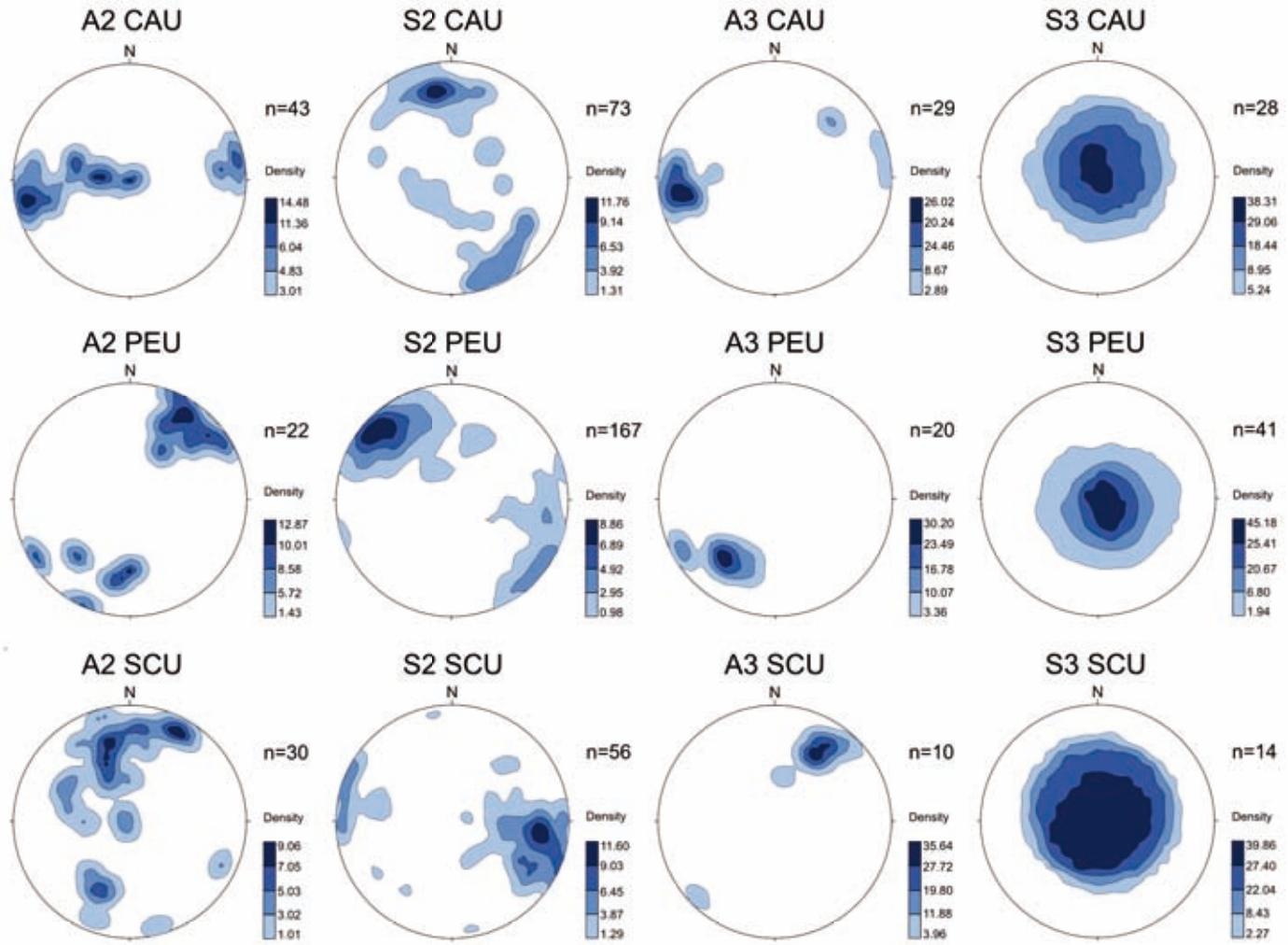

Figure 8

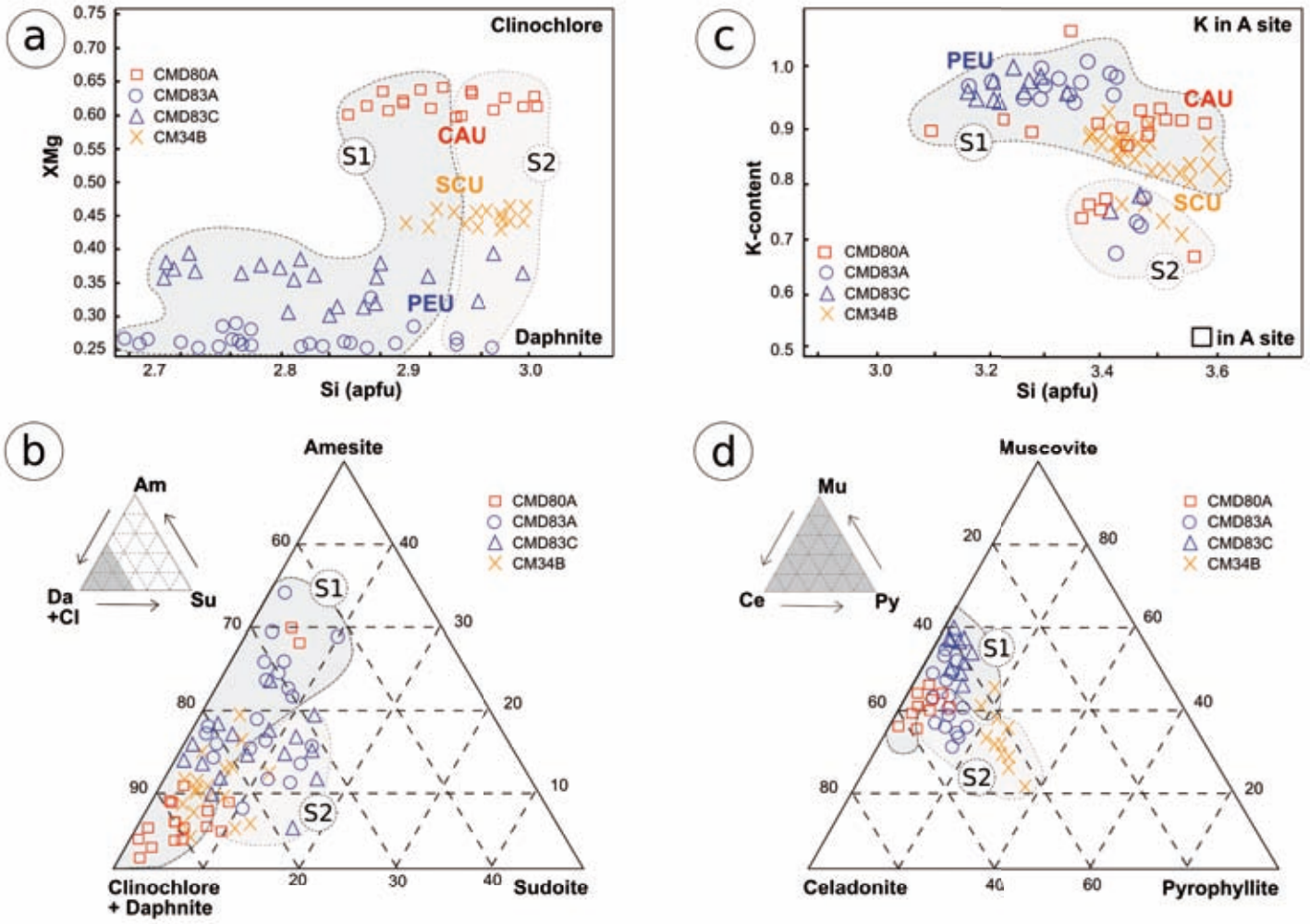

Figure 9

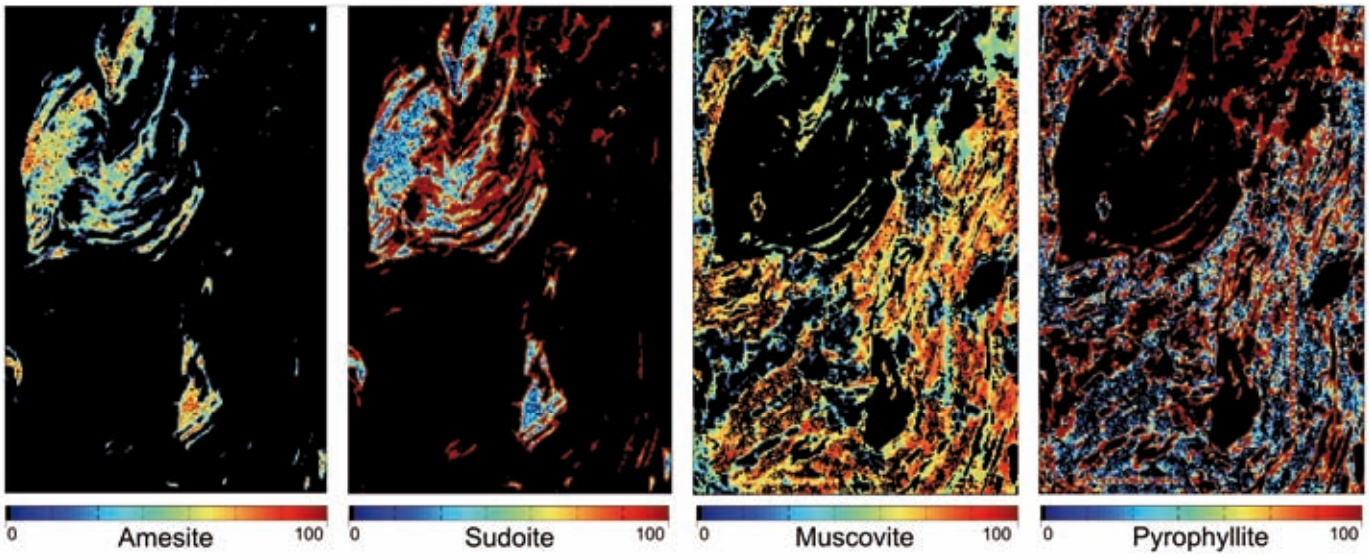

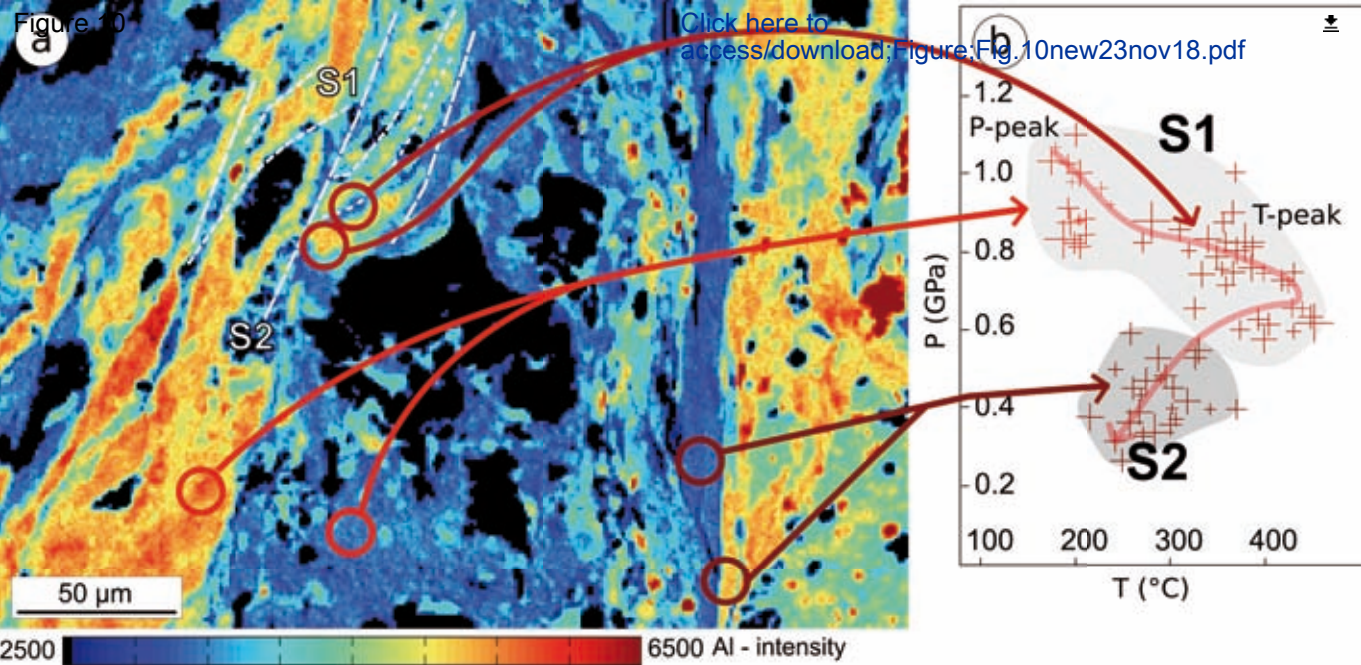

Table 1

	D1	D2	D3
Mapscale	-	F2 megafolds (e.g. the syncline of Cima Pedani, PEU)	F3 open to close folds that fold also the tectonic contacts between CAU, PEU, SCU and LEU
Mesoscale	Relics of S1 foliation within S2 foliation (only in the Laminated Metalimestone Fm. of PEU), S1 foliation in the hinges zone of F2 folds	F2 folds (isoclinal, non-cylindrical) with related S2 axial plane foliation (NE-SW general trend), well observed in all the lithotypes and classified as coarse-grained, continued schistosity; A2 axes (scattered)	Cylindrical open to close F3 folds associated with S3 sub-horizontal axial plane foliation; S2 and S3 foliations are coaxial; A3 axes dipping to NE/W-SW
Microscale	S1 foliation preserved in the pelitic layer of Metavolcanic and Metavolcaniclastic Fm., Laminated Metalimestone Fm., Metabreccia and Metasandstone Fm. of CAU, PEU and SCU.	In metapelites: S2 foliation that transposes (along the flanks of F2 folds) or crenulates (in the hinges of F2 folds) the S1 foliation; in metagranitoids: S2 foliation defined by the dynamic recrystallization of quartz and feldspar. S-C fabric and σ-type porphyroclasts (top-to-NW sense of shear)	S3 foliation classifiable as crenulation cleavage in metapelites and metasandstones and as disjunctive cleavage in metagranitoids and metalimestones
Metamorphic assemblage (metapelites)	Chlorite + phengite + albite + quartz + opaque oxides ± k-feldspar ± calcite ± epidote, allanite, titanite and monazite.	Chlorite + phengite + quartz + feldspars + calcite (thinner than those grew during the D1).	Minor recrystallization of quartz, calcite and opaque oxides
Samples	CMD80A (CAU); CH31 and CMD83A,C, (PEU); CM34B, CH55 (SCU)	CH2, CH51, CMD80A (CAU); CH50, CMD83A,C, (PEU); CM34B, CH55 (SCU)	CH51 (CAU)

Table 2

Tab.2 EPMA analysis of the chlorite-phengite couples.

Sample	CMD80A (Canavaggia Unit)						CMD83A (Pedani Unit)						CM34B (Scoltola Unit)					
Domain	S1 (HP)		S1 (HT)		S2		S1 (HP)		S1 (HT)		S2		S1 (HP)		S1 (HT)		S2	
Mineral	*Chl70*	*Phg67*	*Chl16*	*Phg43*	*Chl19*	*Phg72*	*Chl2*	*Phg5*	*Chl8*	*Phg1*	*Chl10*	*Phg2*	*Chl1*	*Phg10*	*Chl6*	*Phg8*	*Chl5*	*Phg7*
Wt%																		
SiO_2	25.94	51.57	27.26	52.70	27.68	51.28	23.35	49.63	23.06	47.54	24.23	50.59	24.14	55.90	26.42	50.93	27.33	51.27
TiO_2	0.01	0.05	0.01	0.06	0.01	0.06	0.07	0.18	0.03	0.14	2.26	0.43	0.04	0.06	0.03	0.05	0.04	0.06
Al_2O_3	18.87	26.81	17.31	25.42	17.75	24.07	19.85	22.91	15.70	26.61	16.53	23.08	17.57	24.29	16.47	24.65	16.60	24.22
FeO	21.76	4.02	22.24	4.23	22.69	4.31	31.70	9.43	31.37	8.91	32.07	6.57	27.82	4.53	27.10	5.07	27.08	4.68
MnO	0.42	0.04	0.42	0.04	0.37	0.03	0.79	0.09	0.29	0.05	0.46	0.08	0.25	0.05	0.56	0.06	0.38	0.04
MgO	15.91	3.49	18.58	3.82	18.15	4.19	10.24	2.85	5.01	1.91	7.11	2.37	11.79	3.79	12.32	3.82	12.47	3.71
CaO	0.15	0.07	0.21	0.08	0.13	0.08	0.08	0.06	0.25	0.06	0.10	0.23	0.11	0.03	0.13	0.03	0.13	0.03
Na_2O	0.04	0.04	0.04	0.05	0.03	0.05	0.02	0.15	0.06	0.06	0.02	0.45	0.02	0.02	0.02	0.02	0.02	0.02
K_2O	0.05	10.38	0.08	8.53	0.06	14.34	0.09	10.00	0.31	10.85	0.18	8.68	0.38	8.39	0.41	8.28	0.46	8.27
Total	83.15	96.46	86.15	94.94	86.87	98.41	86.19	95.30	76.06	96.13	82,96	92.48	82.12	97.05	82.45	92,90	84.51	92.29
Cations																		
Si	2.84	3.42	2.88	3.51	2.91	3.43	2.63	3.44	2.98	3.27	2.85	3.52	2.80	3.62	2.92	3.48	3.04	3.52
Ti	-	-	-	-	-	-	0.01	0.01	-	0.01	0.20	0.02	-	-	-	-	-	-
Al	2.44	2.10	2.16	2.00	2.20	1.90	2.63	1.87	2.39	2.16	2.29	1.89	2.40	1.86	2.23	1.99	2.17	1.96
Fe^{2+}	1.99	0.22	1,97	0.34	1.99	0.24	2.98	0.55	3.39	0.51	3.15	0.38	2.70	0.25	2.60	0.29	2.52	0.27
Mn	0.04	-	0.04	-	0.03	-	0.08	0.01	0.03	-	0.05	0.01	0.03	-	0.05	-	0.04	-
Mg	2.59	0.35	2.94	0.38	2.84	0.42	1.72	0.29	0.97	0.20	1.25	0.25	2.04	0.37	2.11	0.39	2.06	0.38
Ca	0.03	-	0.02	-	0.02	0.01	0.01	-	0.04	-	0.01	0,02	0.01	-	0.02	-	0.01	-
Na	-	-	0.01	0.01	0,01	0.01	-	0.02	0.01	0.01	0.01	0.06	-	-	-	-	-	-
K	0.01	0.88	0.01	0.72	0.01	1.22	0.01	0.88	0.05	0.95	0.03	0.77	0.06	0.69	0.06	0.72	0.07	0.72
Sum OX	14	11	14	11	14	11	14	11	14	11	14	11	14	11	14	11	14	11

- : below detection limits.

Table 3

Tab. 3. P-T conditions of the studied samples obtained with the chlorite-phengite-quartz-water multi-equilibrium approach (Vidal and Parra, 2000).

	Chl-Phg-Qtz-Wtr multi-equilibrium approach		
	P-peak	T-peak	S2
CAU	0.82-1.04 GPa, 176-262°C	0.63-0.76 GPa, 393-455°C	0.33-0.45 GPa, 247-310°C
PEU	0.8-1.35 GPa, 280-360°C	0.45-0.75 GPa, 435-440°C	0.23-0.35 GPa, 237-351°C
SCU	0.9-1.34 GPa, 277-280°C	0.51-0.83 GPa, 388-435°C	0.26-0.31 GPa, 278-312°C
LEU	*0.93 GPa, 380°C*	*0.7 GPa, 450°C*	

Figure 11

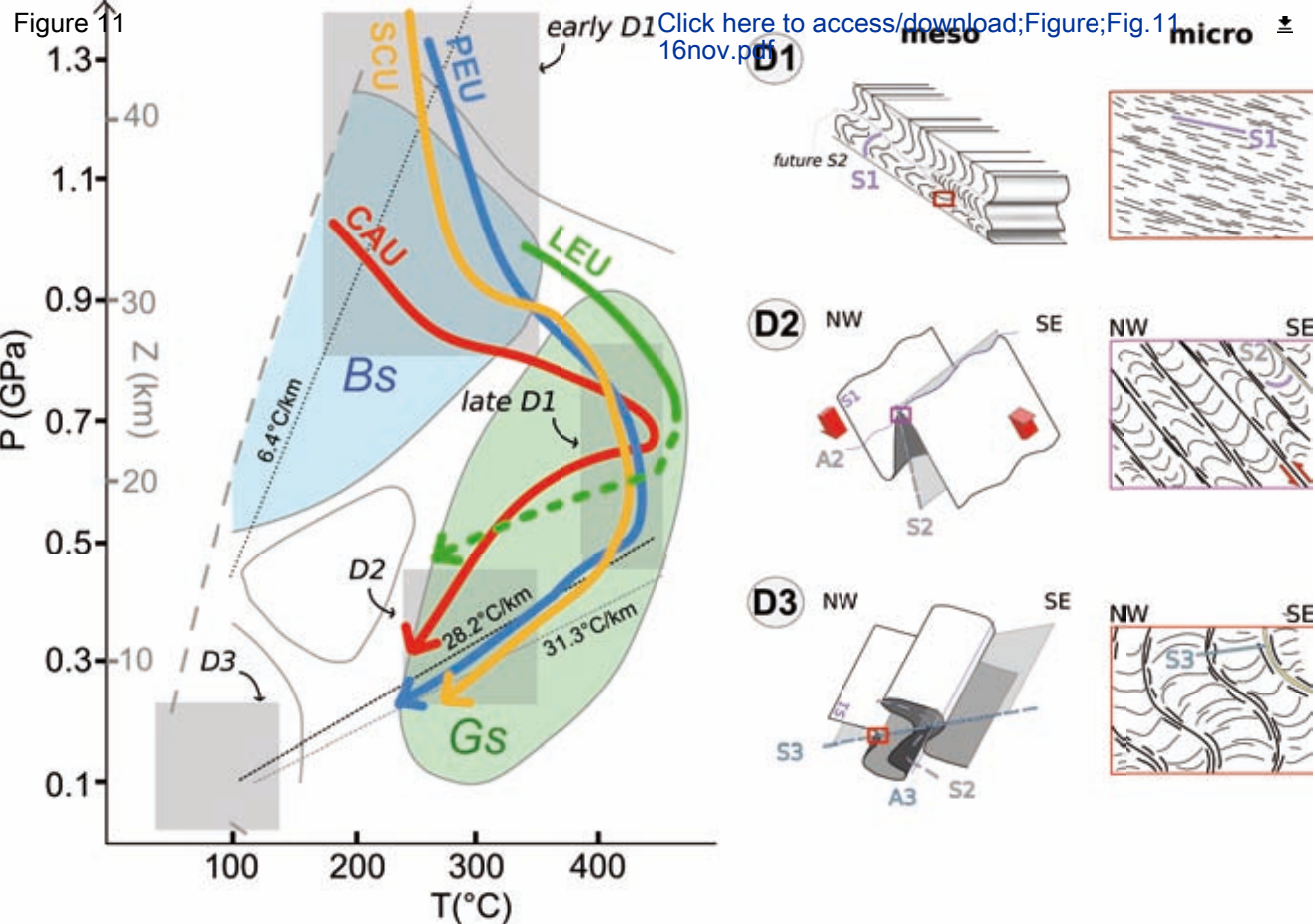

Figure 12

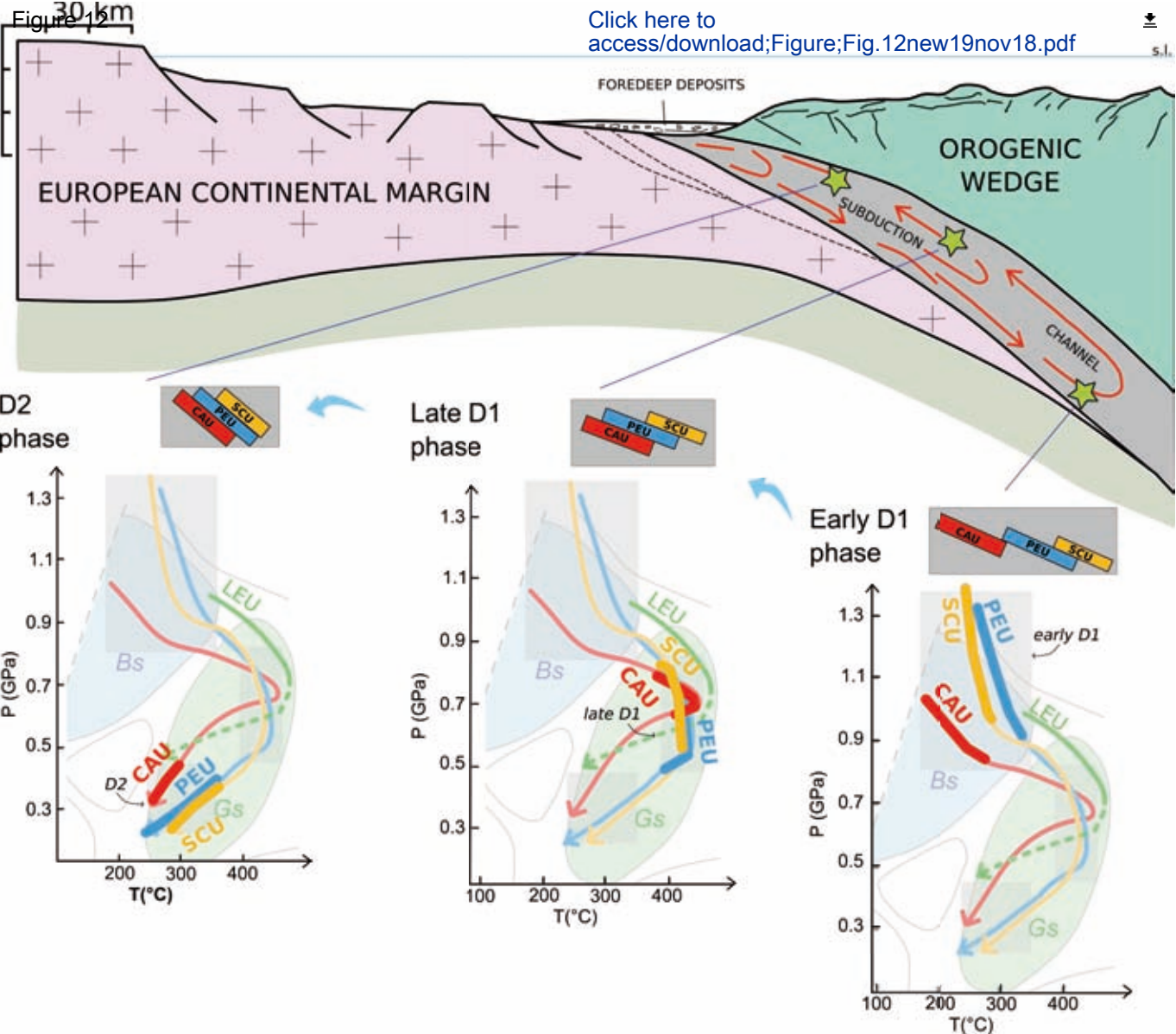

Figure 13